Smart Structures and Systems, *Vol. 33, No. 6 (2024) 465-482*
https://doi.org/10.12989/sss.2024.33.6.465

Robust wireless sensor network configuration design for structural health monitoring with optimal information-energy tradeoff

Xiao-Han Hao [1a], Sin-Chi Kuok [2,3b] and Ka-Veng Yuen*[2,3]

[1] *School of Safety Engineering and Emergency Management, Shijiazhuang Tiedao University, Shijiazhuang 050043, China*
[2] *State Key Laboratory of Internet of Things for Smart City and Department of Civil and Environmental Engineering, University of Macau, Macao SAR, China*
[3] *Guangdong-Hong Kong-Macau Joint Laboratory for Smart Cities, University of Macau, Macao SAR, China*

(*Received April 9, 2023, Revised October 20, 2023, Accepted August 23, 2024*)

Abstract. In this paper, a robust wireless sensor network configuration design method is proposed to develop the optimal configuration under the consideration of sensor failure and energy consumption. A malfunctioned sensor in a wireless sensor network may lead to data transmission failure of the entire sensing cluster, inducing severe deterioration in system identification performance. The proposed method determines a wireless sensor network configuration that is robust against sensor failure. By utilizing Bayesian inference, we introduce a robust indicator to evaluate the impact on estimation accuracy of sensor configurations with various malfunctioned sensors. Moreover, a network formation strategy is proposed to optimize the energy efficiency of the wireless sensor network configuration. Therefore, the resultant robust wireless sensor network configuration can operate with the minimum energy consumption while the measurement information of the sensor network with malfunctioned sensors can be guaranteed. The proposed method is illustrated by designing the robust wireless sensor network configurations of a truss model and a bridge model.

Keywords: Bayesian inference; energy efficiency; multi-type sensing devices; parameter identification; robust wireless sensor network; sensor failure

1. Introduction

Nondestructive structural health monitoring using measurable structural response has attracted increasing attention for decades (Noori *et al*. 2010, Casciati and Fuggini 2011, Zhang *et al*. 2016, Zhao *et al*. 2018, Lei *et al*. 2021). It aims to diagnose and prognose the structural health condition of operating structures (Lei *et al*. 2017, 2020, Lam *et al*. 2018, Yi *et al*. 2019, Zhang *et al*. 2019). Along with the rapid development of wireless sensing technology in recent years, wireless sensor networks become the flexible alternative for structural health monitoring of civil engineering infrastructures (Spencer and Cho 2011, Kuok and Yuen 2012, Fu *et al*. 2013, Hao *et al*. 2022a, Zhou *et al*. 2023). Compare to traditional wire sensor networks, wireless sensor networks are flexible to deploy and wireless data transmission is more cost effective. In practice, sensor location and quantity can seriously affect the performance of structural health monitoring. Extensive research efforts have been devoted to sensor placement design (Kammer 1991, Udwadia 1994, Stephan 2012, Li *et al*. 2017, Argyris *et al*. 2018, Zhang *et al*. 2023, Ercan *et al*. 2023). The four major categories are information-based method (Shi *et al*. 2020), energy-based method (Papadopoulos and Garcia 1998), response reconstruction-based method (Yao *et al*. 1993), and modal parameters-based method (Reynier and Abou-Kandil 1999). As a flourishing branch of the information-based method, information entropy has been widely used by researchers (Yuen *et al*. 2001, Papadimitriou and Lombaert 2012, Yuen and Kuok 2015, Ercan and Papadimitriou 2021, Yuen *et al*. 2022, Lam and Adeagbo 2022). On the other hand, since wireless sensors commonly encounter power restrictions, operating energy consumption is also a core element that should be considered in the wireless sensor network configuration design (Spencer *et al*. 2004, Sengupta *et al*. 2013, Al-Turjman *et al*. 2015, Elhabyan *et al*. 2019, Tan and Zhang 2020). Increasing the sensors provides more information but consumes higher energy. However, decreasing the sensors can reduce the required energy but the captured information may not be sufficient to provide satisfactory performance on system identification. To achieve the best tradeoff between estimation accuracy and energy efficiency, wireless sensor network configuration optimization methods have been proposed in the literature (Li *et al*. 2010, Onoufriou *et al*. 2012, Zhou and Yi 2013, Jalsan *et al*. 2014, Bhuiyan and Cao 2015, Zhou *et al*. 2015, Elsersy *et al*. 2016, El-Qawasma *et al*. 2019). Onoufriou *et al*. (2012) employed the determinant of Fisher information matrix to quantify the information quality and considered the energy consumption in the wireless sensor placement design. Fu *et al*. (2013) used the eigensystem realization

*Corresponding author, Ph.D., Distinguished Professor, E-mail: kvyuen@um.edu.mo
[a] Ph.D., Lecturer
[b] Ph.D., Assistant Professor

ISSN: 1738-1584 (Print), 1738-1991 (Online)

algorithm to perform the modal analysis and constructed the energy-balanced routing tree to evaluate the energy consumption for selecting the optimal wireless sensor placement. Jalsan *et al*. (2014) obtained the Pareto optimal solution set for the wireless sensor layout optimization problem with considering the information quality and the energy consumption. Bhuiyan and Cao (2015) optimized the wireless sensor placement for structural health monitoring to satisfy the civil engineering requirement and prolong the lifetime of the wireless network. Elsersy *et al*. (2016) utilized the mixed integer programming modeling to solve the joint optimization of the wireless sensor location, routing, and flow assignment. Zhou et al. (2019, 2021) considered the information effectiveness and energy consumption combined with the network connectivity in the wireless sensor placement optimization.

To establish the connections between the components in a wireless sensor network, the cluster-based network is a widely used hierarchical configuration with high scalability. The sensors in the cluster-based network are divided into different clusters. Each cluster selects one sensor as the cluster head node that collects the measurements from all the sensors in the cluster, aggregates the data and transmits the aggregated data to the base station. The cluster-based network is energy efficient since it reduces the total transmission distance of the network components (Hao *et al*. 2022b). Liu *et al*. (2011) proposed a cluster-based modal analysis strategy to design the wireless sensor network configuration with high information effectiveness and energy efficiency. In Hu *et al*. (2012), a distributed damage detection method was modified to enhance the identify-cation accuracy and improve the network performance of the wireless sensor network configuration. A sensor deployment framework based on the cluster-tree network was proposed for determining the optimal design with multi-type wireless sensors (Liu *et al*. 2016). Fang *et al*. (2018) took the modal information quality and the energy consumption into consideration to determine the optimal number and locations for sensors. Geoffrine and Geetha (2019) optimized the energy efficiency of wireless sensor placement by clustering the sensor nodes with locations determined using exhaustive search.

Despite the widespread investigation of optimizing the wireless sensor placement, the robustness of the configurations under possible sensor failures has been neglected. In practice, one-sensor failure is commonly encountered in long-term sensory monitoring systems (Yuen *et al*. 2022). Sensor failure will lead to the reduction of the information extracted from measurements (Li *et al*. 2019, Huynh *et al*. 2020, Aswal *et al*. 2022, Jana *et al*. 2022, Zhang *et al*. 2022, Huang *et al*. 2022). Yuen *et al*. (2022) verified that the estimation accuracy of the optimal sensor configuration decreases under sensor failure. In contrast to sensor placement in wired networks, the performance of wireless sensor placement can be more susceptible to sensor failure. In the cluster-based network, a cluster head node transfers the data from all sensors in the cluster to the base station. Therefore, if a cluster head is out of order, data transmission of the corresponding non-cluster head nodes in the same cluster will be affected. As a result, the identification performance of the wireless sensor network configuration will be substantially degraded under sensor failure. Therefore, it is of practical value to develop a robust wireless sensor placement method.

In this study, an energy-aware robust wireless sensor network configuration method is proposed. By utilizing Bayesian inference, a robust indicator is introduced to evaluate the performance of wireless sensor networks with malfunctioned devices. The indicator quantifies the estimation uncertainty regarding the sensor locations. When any of the sensing devices become malfunctioned, the information of the affected sensors will be lost and the data-transmission of the associated cluster will be changed. The proposed method develops the optimal configuration under the worst possible malfunctioned scenario. Since the proposed indicator provides a holistic factor without constraints on the sensor types, the proposed method is applicable to structural health monitoring of large-scale civil engineering infrastructures that the wireless sensor network composes of versatile types of sensors. Moreover, a network formation strategy is proposed to establish the most energy-efficient sensor network configuration that achieves the required estimation accuracy.

This paper is organized as follows. Section 2 describes the concerned problem for wireless sensor network configuration with the consideration of possible sensor failure. Section 3 presents the formulation of network performance evaluation. Then, in Section 4, we present the network formation scheme. In Section 5, the procedure and major contributions of the proposed method are summarized. In Section 6, applications to a truss model and a bridge model are demonstrated.

2. Problem description

In this study, a wireless sensor network configuration design method for robust and energy-efficient design is proposed. The resultant wireless sensor network configuration is robust against sensor failure. Moreover, it operates with the minimum energy consumption while the quality of the measurement information can be guaranteed. In wireless sensor network design, sparsely distributed sensors can better capture the overall information of the structure but consume more energy for data transmission. In contrast, although closely distributed sensors consume less energy, they may provide redundant information about part of the structure but incomplete information for the rest. Therefore, it is essential to develop the wireless sensor configuration with the optimal tradeoff between the information gain and energy consumption. Assume that a wireless sensor network with $N_{\mathcal{T}}$ types of sensors is utilized to monitor the structural response of the target dynamical system. For the τth type of sensor, $\boldsymbol{\mathcal{P}}_\tau$ denotes their possible locations for installation. The corresponding sensor locations of the wireless sensor network can be expressed as $\mathbf{L} = \bigcup_{\tau=1}^{N_{\mathcal{T}}} \mathbf{L}_\tau = \bigcup_{\tau=1}^{N_{\mathcal{T}}} \{l_{\tau,\nu}, \nu = 1,2,\dots,N_\tau\}$, where N_τ is the number of the τth type of sensor; and $l_{\tau,\nu} \in \boldsymbol{\mathcal{P}}_\tau$ represents the location at which the νth sensor of τth type. Herein, the total number of sensors is $N_L = \sum_{\tau=1}^{N_{\mathcal{T}}} N_\tau$. Use $\mathbf{W_L}$ to denote the routing configuration that

specifies the data transmission routes between the base station and the sensor nodes placed at $\mathbf{L}$. The sensors are grouped into different clusters and each cluster contains a single type of sensor. In each cluster, one of the sensors acts as the cluster head node while other sensors are non-cluster head nodes. The cluster head node collects the measurement from all non-cluster head nodes in the associated cluster and transmits the aggregated measurement to the base station.

To ensure the robustness of the sensor network, the worst one-sensor failure scenario is considered to design the robust sensor network configuration. In the design stage, it is unable to predict which sensor node will fail during long-term monitoring. A malfunctioned sensor may lead to two possible situations regarding the change of data transmission. The first one refers to a non-cluster head node failure. In this situation, the corresponding measurement of the malfunctioning sensing channel becomes unavailable. The second one refers to a cluster head node failure. Since the cluster head node is responsible for transferring the aggregated measurements to the base station, its failure also affects the data transmission of the non-cluster head nodes in the same cluster. For such a situation, the measurements of the associated non-cluster head nodes will be sent to the nearest operating cluster head of the same sensor type. However, if a non-cluster head node is placed at a location that exceeds the cluster detection radius R_c from any cluster head of the same sensor type, the measurement of this sensing channel will not reach the base station. To maximize the usage of the well-functioning sensors, cautious design on the robustness of the sensor network configuration is essential.

In this study, the performance of a wireless sensor network configuration is evaluated by the maximum coefficient of variation (COV) of the identified parameters obtained from the captured measurement. Given the sensors with locations specified by $\mathbf{L}$, the maximum COV is denoted as $\zeta_{\mathbf{L}}^{\mathcal{M}}$. Assume that the kth sensor in $\mathbf{L}$ is out of order. The corresponding maximum COV is denoted as $\zeta_{\Phi_{-k}(\mathbf{L})}^{\mathcal{M}}$, where the subscript $-k$ in $\Phi_{-k}(\mathbf{L})$ indicates the kth sensor in $\mathbf{L}$ is removed. To have the conservative design, the worst one-sensor failure configuration is utilized. For this purpose, the robust maximum COV obtained by the sensors with $\mathbf{L}$ is defined as

$$\zeta_{\mathbf{L}}^{\mathcal{M}R} = \max_{k=1,2,\ldots,N_L} \zeta_{\Phi_{-k}(\mathbf{L})}^{\mathcal{M}} \tag{1}$$

It indicates that the sensor configuration with the highest $\zeta_{\Phi_{-k}(\mathbf{L})}^{\mathcal{M}}$ among all possible one-sensor failure configurations is used for the design. The robust maximum COV evaluates the information effectiveness of the sensors with $\mathbf{L}$. In addition, to achieve the optimal information-energy cost tradeoff, the wireless sensor network is designed to operate with the minimum energy consumption while guarantee the quality of the measurement information of the sensor network with malfunctioned sensors. Therefore, the wireless sensor placement optimization problem can be formulated as

$$\min_{\mathbf{L}} E(\mathbf{W}_{\mathbf{L}}) \quad \text{subject to} \quad \zeta_{\mathbf{L}}^{\mathcal{M}R} \le \bar{\zeta} \tag{2}$$

where $E(\mathbf{W}_{\mathbf{L}})$ is the energy consumption of the network configuration $\mathbf{W}_{\mathbf{L}}$; and $\bar{\zeta}$ is the allowable COV of the identified parameters. For the situation with additional malfunctioned sensors, the COV with the associated number of malfunctioned sensors can be considered.

For a large-scale infrastructure, the number of possible sensor network configurations can be huge so the computational cost of all possible configurations can be expensive or even prohibitive. To reduce the computational cost, genetic algorithm (GA) (Liu *et al*. 2008, Yi *et al*. 2011) is implemented for solving the optimization problem in an iterative manner. The main procedure of GA is briefed as follows. First, N_p initial populations are generated. For the gth generation, the collection of the generated N_p different N_L-sensor configurations is denoted as $\mathbb{L}_g = \{\mathbf{L}_{g,1}, \mathbf{L}_{g,2}, \ldots, \mathbf{L}_{g,N_p}\}$. In particular, the initial generation is associated with $g = 0$. Then, the performance of each candidate in $\mathbb{L}_g$ can be evaluated by using the function optimization criteria given by Eq. (2). Finally, the initial population evolves through generations until the absolute percentage change in the energy consumption is less than the acceptable tolerance δ_T (e.g., 0.01%). The generational evolution involves natural selection, crossover and mutation. The natural selection is a process of selecting the parent designs for further reproductive operations based on the energy efficiency ranking of the current populations. The crossover process creates two offspring designs by exchanging some parts of the bit-string representations of the two parent designs. The mutation is a random process to change the bit value within the generated strings. The resultant design is the one with the minimum energy consumption. In the following, we will present the formulation of the network performance evaluation.

3. Network performance evaluation

In this work, both the estimation performance and the energy consumption are considered in the robust wireless sensor network design. In this section, we will present the formulation of the quantification of estimation uncertainty based on the measurement captured by the available sensors and the energy consumption of different components in the wireless sensor network.

3.1 Network estimation accuracy

Consider a linear dynamical model with N_d DOFs and the equation of motion

$$\mathbf{M}(\boldsymbol{\theta}_M)\ddot{\mathbf{y}}(t) + \mathbf{C}(\boldsymbol{\theta}_M)\dot{\mathbf{y}}(t) + \mathbf{K}(\boldsymbol{\theta}_M)\mathbf{y}(t) = \mathbf{V}\mathbf{F}(t) \tag{3}$$

where $\mathbf{M}(\boldsymbol{\theta}_M) \in \mathbb{R}^{N_d \times N_d}$, $\mathbf{C}(\boldsymbol{\theta}_M) \in \mathbb{R}^{N_d \times N_d}$ and $\mathbf{K}(\boldsymbol{\theta}_M) \in \mathbb{R}^{N_d \times N_d}$ are the mass, damping and stiffness matrix, respectively; $\boldsymbol{\theta}_M$ is the structural model parameter vector; $\mathbf{F}(t) \in \mathbb{R}^{N_F}$ is the excitation applied to the structure at time t; $\mathbf{V} \in \mathbb{R}^{N_d \times N_F}$ is the excitation distributing matrix; and $\mathbf{y}(t)$ is the displacement vector of the structure. Let the instrumented response vector be $\mathbf{x}(t) = \mathbf{T}[\mathbf{y}(t)^T, \dot{\mathbf{y}}(t)^T, \ddot{\mathbf{y}}(t)^T]^T$, where $\mathbf{T} \in \mathbb{R}^{N_X \times 3N_d}$ is the

transformation matrix that maps the system state $[\mathbf{y}(t)^T, \dot{\mathbf{y}}(t)^T, \ddot{\mathbf{y}}(t)^T]^T$ to the observed response $\mathbf{x}(t)$. It contains the measurable structural response using the available versatile sensors. Based on the sensors with $\mathbf{L}$, the measurement at the mth time step $\mathbf{z}_\mathbf{L}(m) \in \mathbb{R}^{N_L}$ is

$$\mathbf{z}_\mathbf{L}(m) = \mathbf{G}(\mathbf{L})\mathbf{x}(m) + \boldsymbol{\varepsilon}_\mathbf{L}(m) \tag{4}$$

where $\mathbf{x}(m)$ is the structural response measured at time $t = m\Delta t$; $\mathbf{G}(\mathbf{L}) \in \mathbb{R}^{N_L \times N_\chi}$ is the observation matrix composed of zeros and ones to select the N_L measured elements in $\mathbf{x}$; and Δt is the sampling time interval. The measurement noise $\boldsymbol{\varepsilon}_\mathbf{L}(m)$ is modeled as a zero-mean Gaussian white noise with the covariance matrix governed by the prediction-error parameter vector $\boldsymbol{\theta}_\varepsilon$. Discrete-time response measurements $D_\mathbf{L} = \{\mathbf{z}_\mathbf{L}(m), m = 1,2,\dots,N_t\}$ are available for N_t time steps. The uncertain parameter vector $\boldsymbol{\theta} = [\boldsymbol{\theta}_M^T, \boldsymbol{\theta}_F^T, \boldsymbol{\theta}_\varepsilon^T]^T \in \mathbb{R}^{N_\theta}$ includes the structural model parameter vector $\boldsymbol{\theta}_M$, the excitation parameter vector $\boldsymbol{\theta}_F$, and the prediction-error parameter vector $\boldsymbol{\theta}_\varepsilon$. By applying the Bayes' theorem, the posterior probability density function (PDF) of the uncertain parameters $\boldsymbol{\theta}$ given the data $D_\mathbf{L}$ can be expressed as (Katafygiotis and Yuen 2001)

$$p(\boldsymbol{\theta}|D_\mathbf{L}) = \kappa_0 p(\boldsymbol{\theta}) p(D_\mathbf{L}|\boldsymbol{\theta}) \tag{5}$$

where κ_0 is a normalizing constant. The prior PDF $p(\boldsymbol{\theta})$ expresses the prior information of the parameters without data. Based on the Bayesian spectral density approach (Katafygiotis and Yuen 2001), the posterior PDF can be obtained. The posterior PDF can be approximated by the Gaussian distribution $\mathcal{N}(\widehat{\boldsymbol{\theta}}_\mathbf{L}, \boldsymbol{\Sigma}_\mathbf{L})$ (Katafygiotis and Yuen 2001). Herein, the optimal parameter vector $\widehat{\boldsymbol{\theta}}_\mathbf{L}$ can be obtained by maximizing the posterior PDF $p(\boldsymbol{\theta}|D_\mathbf{L})$. The covariance matrix $\boldsymbol{\Sigma}_\mathbf{L}$ can be obtained by taking the inverse of the Hessian of the objective function $-\ln[p(\boldsymbol{\theta}|D_\mathbf{L})]$ evaluated at $\boldsymbol{\theta} = \widehat{\boldsymbol{\theta}}_\mathbf{L}$. Consequently, the maximum COV of the parameters is given by

$$\zeta_\mathbf{L}^{\mathcal{M}} = \max_{i=1,2,\dots,N_\theta} \left(\sqrt{\boldsymbol{\Sigma}_\mathbf{L}^{(i,i)}} / \widehat{\boldsymbol{\theta}}_\mathbf{L}^{(i)} \right) \tag{6}$$

where $\widehat{\boldsymbol{\theta}}_\mathbf{L}^{(i)}$ is the ith optimal parameter in $\widehat{\boldsymbol{\theta}}_\mathbf{L}$; and $\boldsymbol{\Sigma}_\mathbf{L}^{(i,i)}$ is the (i,i)th component of the covariance matrix $\boldsymbol{\Sigma}_\mathbf{L}$. The obtained maximum COV represents the estimation accuracy of the identified parameters. In addition to the estimation accuracy of the parameters, energy efficiency is the other core concern for wireless sensory system design. In the following, we will present the formulation for network energy efficiency.

3.2 Network energy efficiency

In the following, we will discuss the consumed energy of the wireless sensor network $\mathbf{W}_\mathbf{L}$. Fig. 1 shows a schematic plot of the representative components in the wireless sensor network. In this figure, the bottom level, middle level, and top level represent the non-cluster head nodes, the cluster head nodes, and the base station, respectively. The locations of a non-cluster head, cluster head, and the base station are denoted as $\bar{l}$, $\hat{l}$, and l', respectively. The dotted arrow represents the data transmission route from a non-cluster head node to a cluster head node while the solid arrow represents the route from a cluster head node to the base station. In each cluster, a non-cluster head node transfers data to its cluster head node. Then, the cluster head node transmits the collected measurement from all sensors in the cluster to the base station.

3.2.1 Energy consumption of non-cluster head

For the nth non-cluster head node of the cth cluster, the consumed energy to transmit $b^{(c)}$ bits of data to the corresponding cluster head is given by Heinzelman *et al.* (2002)

$$\begin{aligned} &E_{\bar{T}n}^{(c)}(\mathbf{W}_\mathbf{L}) = e_T^{(c)} b^{(c)} + a_{\hat{l}}^{(c)} b^{(c)} \hat{d}_{c,n}^{\gamma_l}(\mathbf{W}_\mathbf{L}), \\ &n = 1,2,\dots,N^{(c)}(\mathbf{W}_\mathbf{L}) - 1;\ c = 1,2,\dots,N_{\hat{l}}(\mathbf{W}_\mathbf{L}) \end{aligned} \tag{7}$$

where $e_T^{(c)}$ is the electronic energy coefficient for data transmission; $a_{\hat{l}}^{(c)}$ is the transmitter power amplifier cost coefficient of the non-cluster head node; $\hat{d}_{c,n}(\mathbf{W}_\mathbf{L})$ is the distance between the nth non-cluster head node in the cth cluster and its associated cluster head node; γ_l is the path loss exponent for transmitting data to the cluster head node; $N^{(c)}(\mathbf{W}_\mathbf{L})$ is the number of sensor nodes in the cth cluster; and $N_{\hat{l}}(\mathbf{W}_\mathbf{L})$ is the number of clusters in the network. Therefore, the overall energy consumption of the $N^{(c)}(\mathbf{W}_\mathbf{L}) - 1$ non-cluster head nodes in the cth cluster is

$$E_{\hat{l}}^{(c)}(\mathbf{W}_\mathbf{L}) = \sum_{n=1}^{N^{(c)}(\mathbf{W}_\mathbf{L})-1} E_{\bar{T}n}^{(c)}(\mathbf{W}_\mathbf{L}) \tag{8}$$

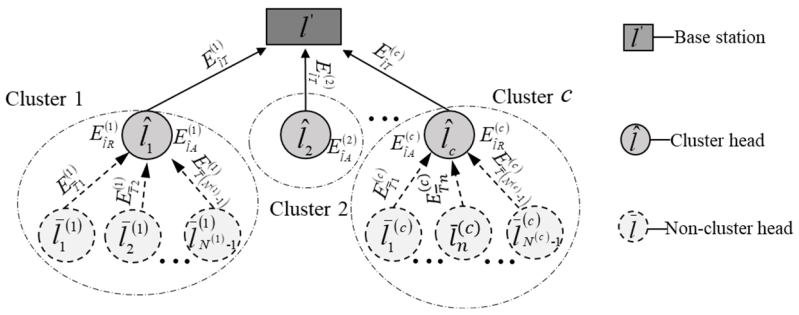

Fig. 1 Schematic plot of the energy consumption of the cluster-based wireless sensor network

As a result, the energy consumption of all the non-cluster head nodes in the entire sensor network can be expressed as

$$E_{\bar{l}}(\mathbf{W_L}) = \sum_{c=1}^{N_{\hat{l}}(\mathbf{W_L})} E_{\bar{l}}^{(c)}(\mathbf{W_L}) \tag{9}$$

3.2.2 Energy consumption of cluster head

The consumed energy of the cluster head node in the c th cluster includes the energy of signal reception $E_{\hat{l}R}^{(c)}(\mathbf{W_L})$, the energy of signal aggregation $E_{\hat{l}A}^{(c)}(\mathbf{W_L})$, and the energy of signal transmission $E_{\hat{l}T}^{(c)}(\mathbf{W_L})$

$$E_{\hat{l}}^{(c)}(\mathbf{W_L}) = E_{\hat{l}R}^{(c)}(\mathbf{W_L}) + E_{\hat{l}A}^{(c)}(\mathbf{W_L}) + E_{\hat{l}T}^{(c)}(\mathbf{W_L}) \tag{10}$$

The three components can be calculated as follows

$$\begin{aligned} E_{\hat{l}R}^{(c)}(\mathbf{W_L}) &= e_R^{(c)} b^{(c)} \left(N^{(c)}(\mathbf{W_L}) - 1\right) \\ E_{\hat{l}A}^{(c)}(\mathbf{W_L}) &= e_A^{(c)} b^{(c)} N^{(c)}(\mathbf{W_L}) \\ E_{\hat{l}T}^{(c)}(\mathbf{W_L}) &= e_T^{(c)} b^{(c)} + a_{\hat{l}}^{(c)} b^{(c)} (d_c'(\mathbf{W_L}))^{\gamma_{l'}} \end{aligned} \tag{11}$$

where $e_R^{(c)}$ is the electronic energy coefficient for data reception of the cth cluster; $e_A^{(c)}$ is the energy coefficient for data aggregation of the c th cluster; $a_{\hat{l}}^{(c)}$ is the transmitter power amplifier cost coefficient of the cth cluster head node; $d_c'(\mathbf{W_L})$ is the distance from the cth cluster head node to the base station; and $\gamma_{l'}$ is the path loss exponent for transmitting data to the base station. Hence, the consumed energy of $N_{\hat{l}}(\mathbf{W_L})$ cluster head nodes in the entire sensor network is

$$E_{\hat{l}}(\mathbf{W_L}) = \sum_{c=1}^{N_{\hat{l}}(\mathbf{W_L})} E_{\hat{l}}^{(c)}(\mathbf{W_L}) \tag{12}$$

Consequently, the overall energy consumption of the network $\mathbf{W_L}$ can be obtained by

$$E(\mathbf{W_L}) = E_{\bar{l}}(\mathbf{W_L}) + E_{\hat{l}}(\mathbf{W_L}) \tag{13}$$

The smaller the value of $E(\mathbf{W_L})$, the less energy consumption the network. In the following, we will present the proposed network formation scheme to optimize the network configuration in the normal function stage and sensor failure stage.

4. Network formation scheme

In this section, we present the strategy to configure the most energy-efficient network $\mathbf{W_L^*}$ regarding the sensor locations $\mathbf{L}$ in the normal function stage. The procedure consists of cluster formation, base station determination, and network formation and evaluation. Then, we present the network reconfiguration to optimize the data transmission of the well-functioning sensors in the sensor failure stage. In particular, two possible sensor failure situations, i.e., cluster head failure and non-cluster head failure, will be considered.

4.1 Energy-efficient network configuration design

The strategy to determine the most energy-efficient network configuration among all possible network configurations based on the sensor locations $\mathbf{L}$ is described as follows. First, all combinations with N cluster heads are constructed by selecting N elements from $\mathbf{L}$, where $N \in \{N_{\mathcal{T}}, N_{\mathcal{T}}+1, \dots, N_L\}$. When $N = N_{\mathcal{T}}$, it means that each cluster head refers to a different sensor type. On the other hand, when $N = N_L$, each cluster contains only one sensor and it acts as the single-cluster head. The locations of the selected N cluster heads are $\hat{\mathbf{L}}^{[N]} = \bigcup_{\tau=1}^{N_{\mathcal{T}}} \hat{\mathbf{L}}_{\tau}^{[N]} = \bigcup_{\tau=1}^{N_{\mathcal{T}}} \left\{\hat{l}_{\tau,\eta}^{[N]}, \eta = 1,2,\dots,N_{\hat{l}_\tau}^{[N]} \geq 1\right\}$, where $\hat{\mathbf{L}}_{\tau}^{[N]} \subset \mathbf{L}_{\tau}$ is a subset of $\mathbf{L}_{\tau}$ and it contains the locations of the cluster head nodes in the τth sensor type. The number of cluster heads of the $N_{\mathcal{T}}$ sensor types fulfills $\sum_{\tau=1}^{N_{\mathcal{T}}} N_{\hat{l}_\tau}^{[N]} = N$. All possible combinations with N cluster heads are included in the set $\hat{\boldsymbol{\mathcal{L}}}^{[N]}$.

Then, the clusters are developed according to the cluster heads located at $\hat{\mathbf{L}}^{[N]}$. Besides of the cluster head nodes, the rest of the sensors in the network are non-cluster head nodes and their locations are indicated by $\bar{\mathbf{L}}^{[N]} = \bigcup_{\tau=1}^{N_{\mathcal{T}}} \bar{\mathbf{L}}_{\tau}^{[N]} = \bigcup_{\tau=1}^{N_{\mathcal{T}}} \left\{\bar{l}_{\tau,\mu}^{[N]}, \mu = 1,2,\dots,N_{\tau} - N_{\hat{l}_\tau}^{[N]}\right\}$, where $\bar{\mathbf{L}}_{\tau}^{[N]} = \mathbf{L}_{\tau} - \hat{\mathbf{L}}_{\tau}^{[N]}$ is the set that contains the locations of the non-cluster head nodes of the τth type of sensor. Each non-cluster head node transmits the measurement to the nearest cluster head node of the same sensor type within the cluster detection radius R_c. For the cluster head at $\hat{l}_{\tau,\eta}^{[N]}$, the locations of its $N_{\bar{l}(\tau,\eta)}^{[N]}$ non-cluster head nodes are denoted as $\bar{l}_{\tau,\eta,\bar{\delta}}^{[N]}$, where $\bar{\delta} = 1,2,\dots,N_{\bar{l}(\tau,\eta)}^{[N]}$. As a result, the locations of the members in the cluster with the cluster head at $\hat{l}_{\tau,\eta}^{[N]}$ can be expressed as $\tilde{\mathbf{L}}_{\tau,\eta}^{[N]} = \left\{\hat{l}_{\tau,\eta}^{[N]}\right\} \cup \left\{\bar{l}_{\tau,\eta,\bar{\delta}}^{[N]}, \bar{\delta} = 1,2,\dots,N_{\bar{l}(\tau,\eta)}^{[N]}\right\}$, where $\left\{\bar{l}_{\tau,\eta,\bar{\delta}}^{[N]},\ \bar{\delta} = 1,2,\dots,N_{\bar{l}(\tau,\eta)}^{[N]}\right\}$ represents the locations of the non-cluster head nodes with the closest cluster head node $\hat{l}_{\tau,\eta}^{[N]}$.

Next, the optimal location of the base station is determined. The base station can be mounted at any nodal location throughout the entire structure. The optimal location of the base station is the one that minimizes the data transmission distances of all network components. Assume that the base station is placed at the φth location and it is denoted as l_{φ}'. The summation of the distances between the base station at l_{φ}' and all cluster head nodes in $\hat{\mathbf{L}}^{[N]}$ is

$$\mathbb{d}_{\varphi}^{[N]} = \sum_{\tau=1}^{N_{\mathcal{T}}} \sum_{\eta=1}^{N_{\hat{l}\tau}^{[N]}} \left(d_{\varphi,(\tau,\eta)}'^{[N]}\right)^{\gamma_{l'}} \tag{14}$$

The optimal location of the base station can be obtained by minimizing $\mathbb{d}_{\varphi}^{[N]}$

$$l'_{\varphi^{*[N]}} = \underset{l'_{\varphi}}{\operatorname{argmin}}\, \mathbb{d}_{\varphi}^{[N]} \tag{15}$$

Thereafter, the corresponding network configuration is formed as $\mathbf{W}_{\hat{\mathbf{L}}^{[N]}} = \left\{ l'_{\varphi^{*[N]}}, \tilde{\mathbf{L}}_{\tau,\eta}^{[N]} \middle| \tau = 1,2,\dots,N_{\mathcal{T}}; \eta = 1,2,\dots,N_{\hat{l}_\tau}^{[N]} \right\}$, where $\tilde{\mathbf{L}}_{\tau,\eta}^{[N]}, \tau = 1,2,\dots,N_{\mathcal{T}}; \eta = 1,2,\dots,N_{\hat{l}_\tau}^{[N]}$ are the locations of the members in the cluster with the cluster head at $\hat{l}_{\tau,\eta}^{[N]}$ and the base station l' associated with the cluster heads at $\hat{\mathbf{L}}^{[N]}$.

Based on the above procedure, the network configurations with N clusters corresponding to all the cluster head combinations in $\hat{\boldsymbol{\mathcal{L}}}^{[N]}$ can be computed. The collection of these network configurations is denoted as $\boldsymbol{\mathcal{W}}_{\hat{\boldsymbol{\mathcal{L}}}^{[N]}} = \left\{ \mathbf{W}_{\hat{\mathbf{L}}^{[N]}} \middle| \hat{\mathbf{L}}^{[N]} \in \hat{\boldsymbol{\mathcal{L}}}^{[N]} \right\}$. By increasing N from $N_{\mathcal{T}}$ to N_L, all possible network configurations with sensor locations $\mathbf{L}$ can be obtained. Finally, the energy consumption of all possible network configurations with sensor locations $\mathbf{L}$ and N cluster heads, where $N \in \{N_{\mathcal{T}}, N_{\mathcal{T}}+1, \dots, N_L\}$, is compared. The network configuration that consumes the minimum energy consumption is selected

$$\mathbf{W}_{\mathbf{L}}^{*} = \underset{\substack{N_{\mathcal{T}} \le N \le N_L \\ \mathbf{W}_{\hat{\mathbf{L}}^{[N]}} \in \boldsymbol{\mathcal{W}}_{\hat{\boldsymbol{\mathcal{L}}}^{[N]}}}}{\operatorname{argmin}} E\left(\mathbf{W}_{\hat{\mathbf{L}}^{[N]}}\right) \tag{16}$$

The resultant $\mathbf{W}_{\mathbf{L}}^{*}$ refers to the most energy-efficient network configuration regarding the sensors located at $\mathbf{L}$ under the condition that all sensors are well-functioning. In the following subsection, the effect of malfunctioned sensors on energy consumption will be discussed.

4.2 Network reconfiguration

When sensor failure occurs, the routing of data transmission will be rearranged to reduce information lost. Since $\mathbf{W}_{\mathbf{L}}^{*}$ is the most energy-efficient network configuration regarding $\mathbf{L}$ with all well-functioning sensors, it is utilized to monitor the structural response of the target dynamical system under the normal function stage. When any sensor malfunctions, the corresponding network will be reconfigured. According to the affected cluster components, a malfunctioned sensor may lead to either non-cluster head failure or cluster head failure. A detailed discussion of the impacts on data transmission and reconfiguration of these two situations are presented as follows.

4.2.1 Cluster head failure situation

Assume that the cluster head node at $\hat{l}_{\tau^\circ,\lambda^\circ}$ in the well-functioning network $\mathbf{W}_{\mathbf{L}}^{*}$ becomes malfunction during the monitoring. Hence, the measurement from all the sensors in the cluster located at $\tilde{\mathbf{L}}_{\tau^\circ,\lambda^\circ}$ cannot be transferred through the original route. In this case, the corresponding non-cluster head nodes with locations $\left\{ \bar{l}_{\tau^\circ,\lambda^\circ,1}, \bar{l}_{\tau^\circ,\lambda^\circ,2}, \dots, \bar{l}_{\tau^\circ,\lambda^\circ,N_{\bar{l}(\tau^\circ,\lambda^\circ)}} \right\}$ will search for the nearest operating cluster head of the same sensor type. Note that if the location of a non-cluster head node exceeds the cluster detection radius R_c of all well-functioning cluster head, this sensor will be detached from the network and its measurement cannot reach the base station. Therefore, the set of locations of the cluster members in the updated clusters can be expressed as

$$\begin{aligned} &\tilde{\mathbf{L}}_{\tau,\lambda}^{u} = \left\{ \hat{l}_{\tau,\lambda} \right\} \cup \left\{ \bar{l}_{\tau,\lambda,\rho^u}^{u}, \rho^u = 1,\dots,N_{\bar{l}(\tau,\lambda)}^{u} \right\}, \\ &\tau = 1,2,\dots,N_{\mathcal{T}}; \lambda = 1,2,\dots,N_{\hat{l}_\tau} \end{aligned} \tag{17}$$

where $N_{\bar{l}(\tau,\lambda)}^{u}$ is the number of the non-cluster head nodes in the updated cluster with $\tilde{\mathbf{L}}_{\tau,\lambda}^{u}$. The value $N_{\bar{l}(\tau,\lambda)}^{u}$ can be different from the number of the non-cluster head $N_{\bar{l}(\tau,\lambda)}$ of the original cluster with $\tilde{\mathbf{L}}_{\tau,\lambda}$. Consequently, the reconfigured network is obtained as

$$\mathbf{W}_{\mathbf{L}}^{*u} = \left\{ l', \tilde{\mathbf{L}}_{\tau,\lambda}^{u} \middle| \tau = 1,2,\dots,N_{\mathcal{T}}; \lambda = 1,2,\dots,N_{\hat{l}_\tau} \right\} \tag{18}$$

If $\tilde{\mathbf{L}}_{\tau^\circ,\lambda^\circ}^{u}$ is an empty set (i.e., $\tilde{\mathbf{L}}_{\tau^\circ,\lambda^\circ}^{u} = \emptyset$), no measurement will be transmitted from the updated cluster to the base station due to the failure of the cluster head node at $\hat{l}_{\tau^\circ,\lambda^\circ}$.

4.2.2 Non-cluster head failure situation

Assume that the non-cluster head node at the location $\bar{l}_{\tau^{\bar\circ},\lambda^{\bar\circ},\rho^{\bar\circ}}$ in the network $\mathbf{W}_{\mathbf{L}}^{*}$ become malfunction. It turns out that the corresponding measurement cannot submit to the cluster head at $\hat{l}_{\tau^{\bar\circ},\lambda^{\bar\circ}}$. Therefore, the locations of the members in the corresponding cluster are updated to exclude the malfunctioned sensor

$$\tilde{\mathbf{L}}_{\tau^{\bar\circ},\lambda^{\bar\circ}}^{u} = \left\{ \hat{l}_{\tau^{\bar\circ},\lambda^{\bar\circ}} \right\} \cup \left\{ \bar{l}_{\tau^{\bar\circ},\lambda^{\bar\circ},1}, \bar{l}_{\tau^{\bar\circ},\lambda^{\bar\circ},2}, \dots, \bar{l}_{\tau^{\bar\circ},\lambda^{\bar\circ},\rho^{\bar\circ}-1}, \bar{l}_{\tau^{\bar\circ},\lambda^{\bar\circ},\rho^{\bar\circ}+1}, \dots, \bar{l}_{\tau^{\bar\circ},\lambda^{\bar\circ},N_{\bar{l}(\tau^{\bar\circ},\lambda^{\bar\circ})}} \right\} \tag{19}$$

In the network, the configuration in other clusters remains the same. It indicates that when $(\tau,\lambda) \neq (\tau^{\bar\circ},\lambda^{\bar\circ})$, $\tilde{\mathbf{L}}_{\tau,\lambda}^{u} = \tilde{\mathbf{L}}_{\tau,\lambda}$, where $\tilde{\mathbf{L}}_{\tau,\lambda}^{u}$ and $\tilde{\mathbf{L}}_{\tau,\lambda}$ are the updated cluster and the original cluster, respectively. Consequently, the reconfigured network is obtained

$$\mathbf{W}_{\mathbf{L}}^{*u} = \left\{ l', \tilde{\mathbf{L}}_{\tau,\lambda}^{u} | \tau = 1,2,\dots,N_{\mathcal{T}}; \lambda = 1,2,\dots,N_{\hat{l}_\tau} \right\} \tag{20}$$

Based on Eqs. (18) and (20), the network reconfigurations of cluster head failure situation and non-cluster head failure situation can be obtained.

4.2.3 Demonstration

In the following, a demonstration of the network reconfiguration with sensor failure is presented. Consider three displacement transducers placed at location 1, 3 and 5, i.e., $\mathbf{L}_1 = \{1,3,5\}$, and seven accelerometers placed at location 7, 9, 11, 13, 15, 17 and 19, i.e., $\mathbf{L}_2 = \{7,9,11,13,15,17,19\}$. Therefore, the corresponding sensor locations of the wireless sensor network is denoted as $\mathbf{L} = \{1,3,5,7,9,11,13,15,17,19\}$. In the same fashion as Fig. 1, Fig. 2 demonstrates the network configurations with all well-functioning sensors and the two-sensor failure

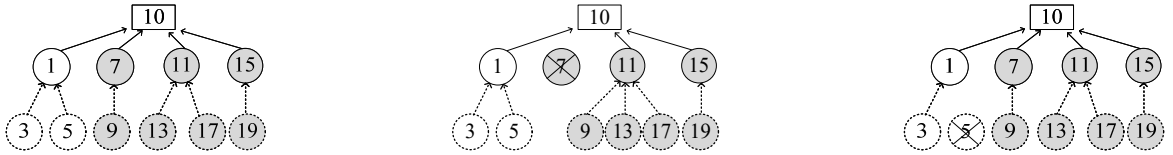

(a) No sensor failure (b) Cluster head failure (c) Non-cluster head failure

Fig. 2 Network configuration

situation. In addition, the white and shaded circular node represent the displacement transducer and accelerometer, respectively. Based on Eq. (16), the most energy-efficient network configuration regarding $\mathbf{L}$ is shown in Fig. 2(a). The base station is placed at location 10. For the case that one of the cluster head nodes (e.g., the accelerometer at location 7) in the network becomes malfunction, the data transmission through this cluster head terminates. The corresponding non-cluster head node (accelerometer at location 9) searches the closest operating cluster head node of the same type (accelerometer at location 11). The reconfigured network is shown as Fig. 2(b). On the other hand, in the case that one of the non-cluster head nodes (e.g., the displacement transducer at location 5) fails, the corresponding measurement of this particular is no longer available but the data transmission of other channels remains unchanged. The reconfigured network is shown in Fig. 2(c).

5. Summary of procedure

The flow chart of the proposed method is shown in Fig. 3 and the procedure is described as follows:

S1. Set $g = 0$, generate the initial population randomly.

S2. Obtain a set of N_p generated sensor configurations to form $\mathbb{L}_g = \left\{\mathbf{L}_{g,1}, \mathbf{L}_{g,2}, \ldots, \mathbf{L}_{g,N_p}\right\}$.

S3. Set $j = 1$.

S4. Determine the energy-efficient network configuration $\mathbf{W}^*_{\mathbf{L}_{g,j}}$ for $\mathbf{L}_{g,j}$ using Eq. (16).

S5. Calculate the robust maximum COV value $\zeta^{\mathcal{MR}}_{\mathbf{L}_{g,j}}$ of the sensors with $\mathbf{L}_{g,j}$ using Eq. (1).

S6. If $\zeta^{\mathcal{MR}}_{\mathbf{L}_{g,j}} \le \bar{\zeta}^R$, go to Step S7; otherwise, remove $\mathbf{L}_{g,j}$ and increase j by 1. Then, repeat the procedure from Step S4. Note that if all sensor configurations cannot achieve the designated allowable COV, a higher allowable COV should be utilized.

S7. Calculate the energy consumption $E\left(\mathbf{W}^*_{\mathbf{L}_{g,j}}\right)$ using Eq. (13).

If $j < N_p$, increase j by 1 and repeat the procedure from Step S4; otherwise, go to Step S8.

S8. Compute the energy consumption of all the configurations in $\mathbb{L}_g$ and obtain the best configuration that minimizes the energy consumption.

S9. If the change of the energy consumption between the best configuration in $\mathbb{L}_g$ and the best offspring design is not larger than the acceptable tolerance (i.e., $\Delta E_{\mathbf{L}^*_g,\mathbf{L}^{o*}_g} = \left|E_{\mathbf{L}^*_g} - E_{\mathbf{L}^{o*}_g}\right| \le \delta_T$, where $E_{\mathbf{L}^*_g}$ and $E_{\mathbf{L}^{o*}_g}$ are the energy consumption of the best configuration $\mathbf{L}^*_g$ and the best offspring design $\mathbf{L}^{o*}_g$, respectively), go to Step S10. Otherwise, perform the evolution of populations. Increase g by 1 and repeat the procedure from Step S2.

S10. Obtain the optimal robust wireless sensor network configuration with N_L sensors using Eq. (2).

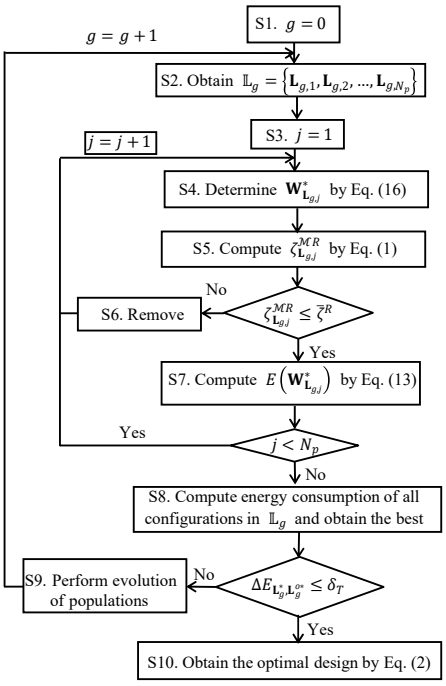

Fig. 3 Flow chart of the proposed method

The two major contributions of this work are summarized as follows:

(1) In this study, an energy-aware robust information entropy-based strategy with the consideration of possible wireless sensor failure is proposed. Despite the widespread investigation of optimizing the wireless sensor placement, the robustness of the configurations under possible sensor failures has been neglected in most existing works. However, in practice, sensor failure is commonly encountered in long-term sensory monitoring systems. Therefore, it is of realistic significance and practical value to develop a robust wireless sensor placement method against malfunctioned sensors.

(2) The proposed method provides valuable information and guidance for general wireless sensor network design in structural health monitoring of large-scale civil engineering infrastructures. Since

the proposed indicator provides a holistic factor without constraints on the sensor types, the proposed method is applicable to the design of wireless sensor networks with versatile sensor types. The resultant optimized design satisfies the designated accuracy requirement with the minimum energy consumption

Table 1 Geometry and material properties of the truss

Parameter	Value
Height of the truss (m)	200
Span length of the bottom of truss (m)	20
Span length of the top of truss (m)	12
Cross-sectional area (m^2)	0.001
Mass density (kg/m^3)	7850
Young's modulus (Pa)	2.0×10^{11}

6. Illustrative examples

In this section, two examples are presented to demonstrate the performance of the proposed method. These examples cover the robust wireless sensor network configuration design for networks with single-type sensors and versatile sensors.

6.1 Example 1: *Truss Model*

A 20-bay truss model (shown in Fig. 4(a)) is considered in this example. The geometry and material properties of the truss are listed in Table 1. The first five nominal natural frequencies are 0.395, 1.799, 3.920, 4.255, and 7.335 Hz. The damping matrix is taken as $\mathbf{C} = \alpha\mathbf{M} + \beta\mathbf{K}$, where α and β are $0.0407\ s^{-1}$ and 1.45×10^{-3} s, respectively. Hence, the damping ratios of the first two modes are 1%. The stiffness matrix $\mathbf{K}$ is parameterized with ten stiffness parameters $\theta_{k1}, \theta_{k2}, \ldots, \theta_{k10}$, where $k_j = \theta_{k1}$, $j = 1,2,\ldots,4$; $k_j = \theta_{k2}$, $j = 5,6$; $k_j = \theta_{k3}$, $j = 7,8,\ldots,12$;

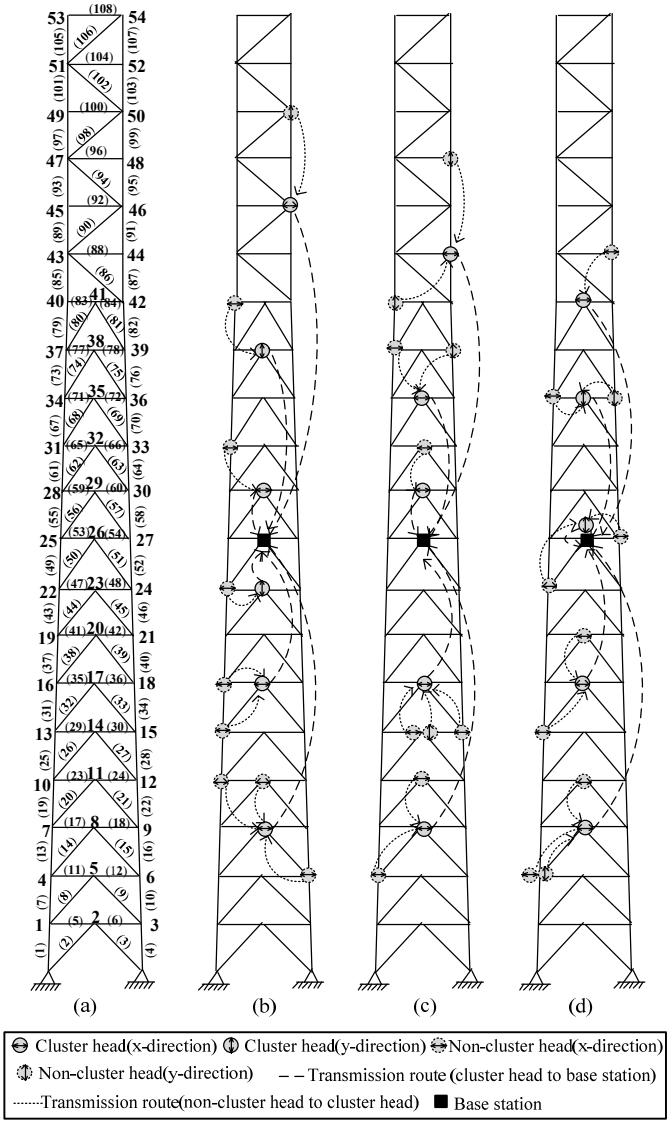

Fig. 4 Truss model (a) the schematic plot; (b) the optimal robust configuration of Case A; (c) the optimal robust configuration of Case B; and (d) the optimal robust configuration of Case C

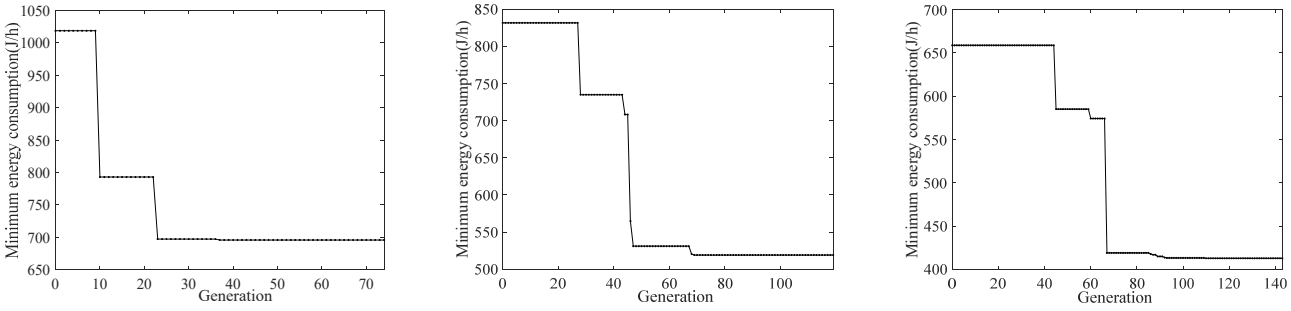

(a) Case A (b) Case B (c) Case C

Fig. 5 Convergence process of the objective function

$k_j = \theta_{k4}$, $j = 13,14,\ldots,18$; $k_j = \theta_{k5}$, $j = 19,20,\ldots,30$; $k_j = \theta_{k6}$, $j = 31,32,\ldots,48$; $k_j = \theta_{k7}$, $j = 49,50,\ldots,66$; $k_j = \theta_{k8}$, $j = 67,68,\ldots,84$; $k_j = \theta_{k9}$, $j = 85,86,\ldots,96$; $k_j = \theta_{k10}$, $j = 97,98,\ldots,108$. For the nominal model, these ten stiffness parameters are equal to unity. The measured structural response consists of horizontal acceleration and vertical acceleration with a sampling rate was 200 Hz. The electronic energy coefficients for data transmission, data reception and data aggregation are $e_T = 45\,\mathrm{nJ/bit}$, $e_R = 135\,\mathrm{nJ/bit}$, and $e_A = 5\,\mathrm{nJ/bit/signal}$, respectively. The cluster radius is $R_c = 20\,\mathrm{m}$ and the number of bits per packet is $4800\,\mathrm{bit/s}$.

6.1.1 Effects of the required parameter estimation accuracy

The effect of the required parameter estimation accuracy on the optimal design is investigated. Robust wireless sensor network configuration design with fifteen accelerometers under three different estimation accuracy requirements is considered. In Case A, B, and C, the allowable COVs of all the estimated parameters are specified as $\bar{\zeta}_A = 1\%$, $\bar{\zeta}_B = 1.5\%$, and $\bar{\zeta}_C = 2\%$, respectively. Fig. 5 shows the convergence process of the objective function of the three cases. It is found that the minimum energy consumption decreases significantly at the early generation state. As the number of generations increases, the minimum energy consumption value converges to a constant.

The resultant optimal robust wireless sensor network configurations are shown in Figs. 4(b)-(d). The square marker, circular marker with a solid border, and circular marker with a dotted border represent the base station, a cluster head node, and a non-cluster head node, respectively. An arrow in the circular marker indicates the monitoring direction of the sensor node. It is observed that the nodal response of the x-direction of the 8th, 11th, and 17th node (i.e., 8-x, 11-x, and 17-x) are common monitoring locations in all three optimal configurations. The optimal robust wireless sensor network configuration of Case A has six clusters while the optimal designs of Case B and Case C have five clusters. For all three configurations, the base station is at the same structural node (i.e., the 26th node). By relaxing the allowable COV value, the distribution of the sensors tends to be more concentrated so that the energy consumption in data transmission can be reduced.

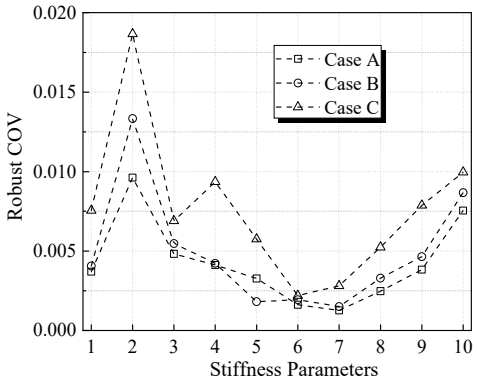

Fig. 6 Robust COVs of the estimated parameters of the optimal robust configurations

For all three resultant configurations, the malfunctioned sensor of the worst case is placed at the x-direction of the 8th node (i.e., 8-x). When this cluster head node becomes malfunction, the corresponding measurement becomes unavailable. Then, the measurements of the non-cluster head node at the x-direction of the 11th node (i.e., 11-x) are sent to the cluster head node placed at the x-direction of the 17th node (i.e., 17-x). However, for Case A, the measurements of the non-cluster heads at the x-direction of the 6th and 10th node (i.e., 6-x and 10-x) cannot submit to any operating cluster head due to the limitation of the cluster detection radius. For the same reason, the measurements of the sensor at the x-direction of the 4th node (i.e., 4-x) in Case B cannot reach the base station. Moreover, the measurements of the sensors at the x-direction and y-direction of the 4th node (i.e., 4-x and 4-y) in Case C cannot be captured.

Fig. 6 shows the resultant robust COVs of the estimated stiffness parameters of the three optimal robust wireless sensor network configurations. It is found that all the optimal configurations with fifteen sensors of the three cases achieved the required estimation accuracy. The estimation accuracy of the optimal design of Case A is the highest among the three optimal configurations. It turns out that the obtained robust COVs of Case A are generally lower than those of the other two cases. The robust maximum COV value of the identified parameters of the optimal design of Case A, B, and C is 0.96%, 1.33%, and

Table 2 Energy consumption of the optimal robust configurations

Case	A	B	C
E (J/h)	695.72	519.33	412.91

1.87%, respectively. According to the results shown in Figs. 5 and 6, all the optimal robust wireless sensor network configurations satisfy the required estimation accuracy with the minimum energy cost.

The resultant energy consumption of the three optimal robust wireless sensor network configurations are shown in Table 2. The lower the allowable COV value, the higher energy consumption of the optimal robust configuration. It is because, under a higher estimation accuracy requirement, fewer possible configurations that satisfy the requirement can be implemented in the optimization. According to the underlying cases, the energy consumed by the optimal robust wireless sensor network configuration of Case A is 695.72 J/h which is 1.7 times of that of the optimal robust configuration of Case C.

6.1.2 Performance of the proposed method

For comparison, the sensor network configuration without the consideration of sensor failure is considered. It is conceptually the same as the proposed method but it does not consider sensor failure. Fig. 7 shows the optimal wireless sensor network configurations with fifteen accelerometers without the consideration of sensor failure. By comparing Figs. 4 and 7, it is found that the optimal designs of the two methods are different. For example, the optimal robust wireless sensor network configuration of Case A obtained by the proposed method is {6-x, 8-x, 10-x, 11-x, 13-x, 16-x, 17-x, 22-x, 23-y, 29-x, 31-x, 38-y, 40-x, 46-x, 50-y} while the optimal design without the consideration of sensor failure is {5-x, 9-x, 11-x, 12-x, 20-x, 24-y, 26-x, 35-y, 36-y, 41-x, 43-y, 45-x, 46-x, 48-x, 50-y}. Except for the sensors at 11-x, 46-x and 50-y, the rest of the twelve sensors are placed at different locations.

Table 3 shows the fifteen-sensor configurations, energy consumption, maximum COV of parameters, and robust

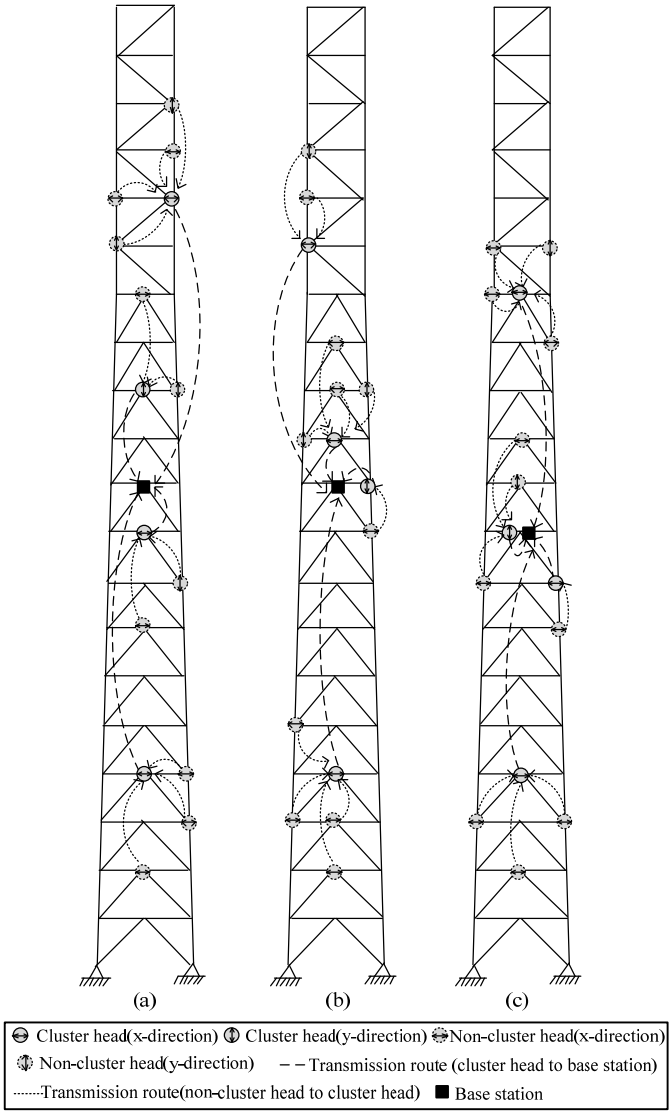

Fig. 7 Optimal configurations without the consideration of sensor failure for (a) Case A; (b) Case B; and (c) Case C

Table 3 Sensor configurations and their resultant properties

Case		Sensor locations	E (J/h)	$\zeta_{\mathbf{L}}^{\mathcal{M}}$	$\zeta_{\mathbf{L}}^{\mathcal{M}R}$
A	$\mathbf{L}_s$	5-x,9-x,11-x,12-x,20-x,24-y,26-x,35-y,36-y,41-x,43-y,45-x,46-x,48-x,50-y	494.28	0.98%	7.45%
	$\mathbf{L}_p$	6-x,8-x,10-x,11-x,13-x,16-x,17-x,22-x,23-y,29-x,31-x,38-y,40-x,46-x,50-y	695.72	0.82%	0.96%
B	$\mathbf{L}_s$	5-x,7-x,8-x,11-x,13-x,27-x,30-y,31-y,32-x,35-x,36-y,38-x,43-x,45-x,47-y	374.43	1.31%	7.81%
	$\mathbf{L}_p$	4-x,8-x,11-x,14-x,14-y,15-x,17-x,29-x,32-x,35-x,37-x,39-y,40-y,44-x,48-y	519.33	0.97%	1.33%
C	$\mathbf{L}_s$	5-x,7-x,9-x,11-x,21-x,22-x,24-x,26-y,29-y,32-x,39-x,40-x,41-x,43-x,44-y	255.40	1.71%	5.18%
	$\mathbf{L}_p$	4-x,4-y,8-x,11-x,13-x,17-x,20-x,22-x,26-y,27-x,34-x,35-y,36-y,41-x,44-x	412.91	1.18%	1.87%

Table 4 Sensor configurations for comparison

Trial		Sensor configurations
1	$\mathbf{L}$	6-x,8-x,10-x,11-x,13-x,16-x,17-x,22-x,23-y,29-x,31-x,38-y,40-x,46-x,50-y
	$\mathbf{W_L}$	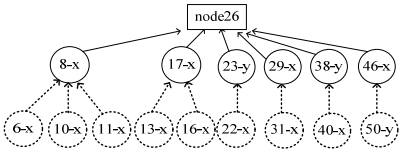
2	$\mathbf{L}$	5-x,9-x,11-x,12-x,20-x,24-y,26-x,35-y,36-y,41-x,43-y,45-x,46-x,48-x,50-y
	$\mathbf{W_L}$	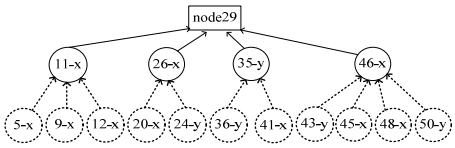
3	$\mathbf{L}$	1-x,5-x,9-x,11-x,13-x,20-x,22-x,26-x,33-x,35-x,40-x,44-x,47-x,51-x,54-x
	$\mathbf{W_L}$	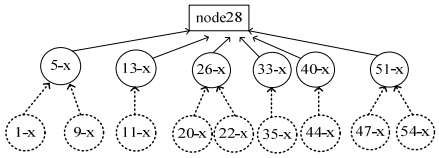
4	$\mathbf{L}$	1-x,2-x,3-x,4-x,5-x,6-x,7-x,8-x,9-x,10-x,11-x,12-x,13-x,14-x,15-x
	$\mathbf{W_L}$	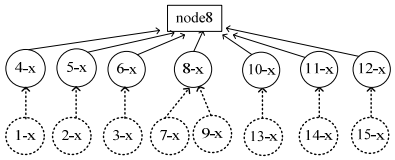
5	$\mathbf{L}$	19-x,20-x,21-x,22-x,23-x,24-x,25-x,26-x,27-x,28-x,29-x,30-x,31-x,32-x,33-x
	$\mathbf{W_L}$	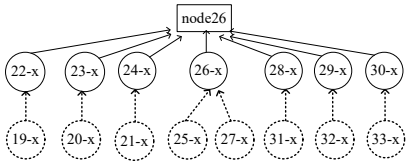
6	$\mathbf{L}$	40-x,41-x,42-x,43-x,44-x,45-x,46-x,47-x,48-x,49-x,50-x,51-x,52-x,53-x,54-x
	$\mathbf{W_L}$	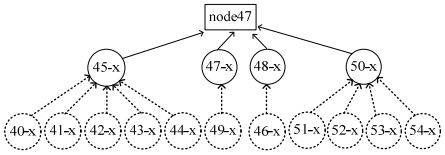

maximum COV of parameters. The three cases with different allowable COV values (i.e., $\bar{\zeta}_A = 1\%$, $\bar{\zeta}_B = 1.5\%$, and $\bar{\zeta}_C = 2\%$) are considered. The designed configuration without the consideration of sensor failure and the proposed optimal robust configuration are denoted as $\mathbf{W}_{\mathbf{L}_s}$ and $\mathbf{W}_{\mathbf{L}_p}$, respectively. For all the three cases, the energy cost of the optimal configuration without the consideration of sensor failure is smaller than that of the optimal robust wireless sensor network configuration. Since the optimal design did not involve any malfunctioned

sensor in the design, the optimal robust wireless sensor network configuration is not the most energy efficient when all sensors are well-functioning. According to the results of the maximum COVs $\zeta_{\mathbf{L}}^{\mathcal{M}}$, the optimal designs of both methods satisfy the required estimation accuracy. However, when any sensors in the network become malfunction, the maximum robust COVs $\zeta_{\mathbf{L}}^{\mathcal{MR}}$ of the optimal configurations without the consideration of sensor failure increase significantly in all the three cases and no longer satisfy the allowable COV. On the other hand, the resultant COVs of the configuration obtained by the proposed method can still fulfill the accuracy requirement regardless of the locations of the malfunctioned sensor. For example, for Case A, the $\zeta_{\mathbf{L}}^{\mathcal{MR}}$ value of $\mathbf{W}_{\mathbf{L}_s}$ is 7.45%, which is 7.8 times of that of $\mathbf{W}_{\mathbf{L}_p}$. It indicates that the optimal robust wireless sensor network configuration is robust against sensor failure.

6.1.3 Verification

In this subsection, the effectiveness of the proposed method is verified. Let the allowable COV value of the estimated parameters be $\bar{\zeta} = 1\%$. For comparison, six configurations with fifteen accelerometers are considered. The sensor locations and network configurations are shown in Table 4. The optimal robust wireless sensor network configuration and the optimal design without the consideration of sensor failure are referred to Trial 1 and Trial 2, respectively. The sensors of Trial 3 were distributed evenly throughout the truss. The accelerometers of Trial 4, 5, and 6 were placed around the bottom, middle, and top part of the truss, respectively. Based on the network formation strategy, the network configurations were obtained and the results are shown in the third column of Table 4.

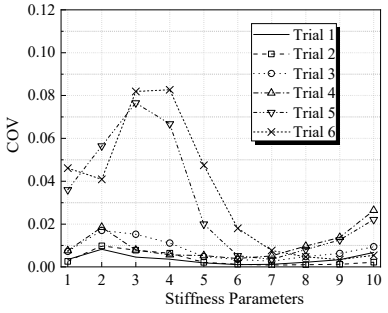

Fig. 8 COVs of the estimated parameters of the six trials for the case without sensor failure

When all sensors in the network are well-functioning, the optimal design obtained by the proposed method can achieve accurate estimation but the energy consumption may not be the lowest. The resultant COVs of the stiffness parameters of the six trials are shown in Fig. 8. From this figure, it is found that except the designed configuration and the optimal design without the consideration of sensor failure, the maximum COVs of the parameters of other trials are larger than 1.0%. Table 5 shows the corresponding energy consumption of the six configurations. The closer the sensors are distributed, the lower the energy is consumed. It is clear that Trial 3 consumed the highest energy among all the concerned configurations. Trial 4, 5 and 6 consumed less energy than the other three trials but their estimation accuracy does not fulfill the requirement. In particular, the maximum COVs of Trial 5 and 6 exceed 7%. The maximum COVs of parameters of Trial 1 and 2 are less than 1%. The energy consumption of the designed robust configuration is 695.72 J/h, which is 1.4 times of the value of Trial 2. This verified that the optimal wireless sensor network configuration obtained without considering sensor failure operates with the minimum energy consumption while the parameter estimation achieves the required accuracy when all the sensors function properly.

Next, we discuss the malfunctioned sensor situation. In particular, the worst one-sensor failure scenario that provides the lowest estimation accuracy is investigated. The reconfigured networks of the six trials are shown in Fig. 9

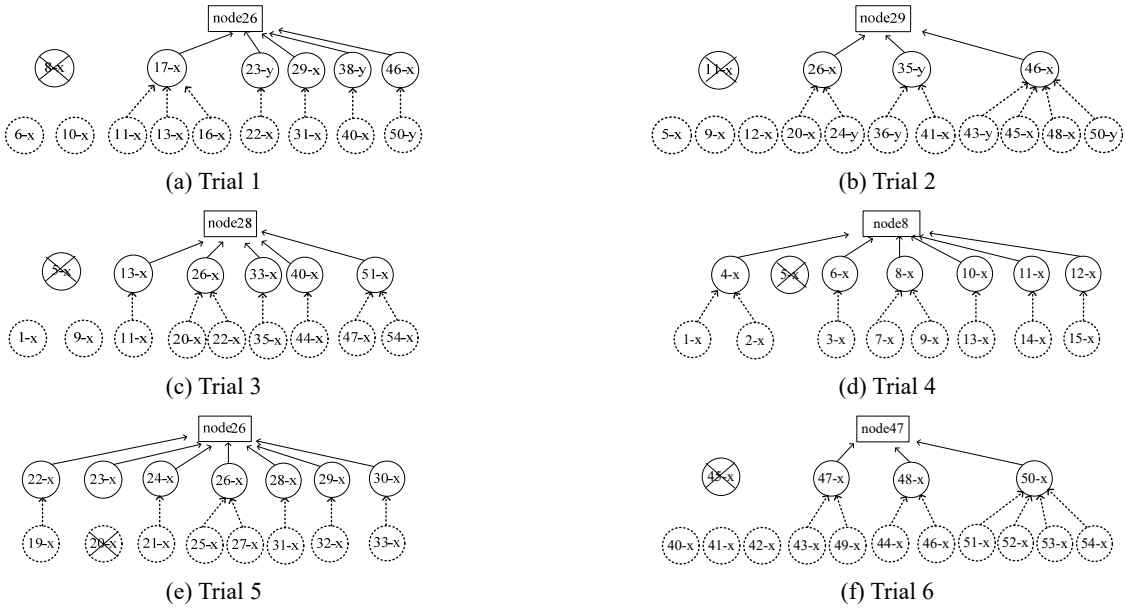

(a) Trial 1 (b) Trial 2

(c) Trial 3 (d) Trial 4

(e) Trial 5 (f) Trial 6

Fig. 9 Reconfigured networks for the six trials

Table 5 Energy consumption of the six trials

Trial	1	2	3	4	5	6
E (J/h)	695.72	494.28	2041.92	34.56	33.84	41.04

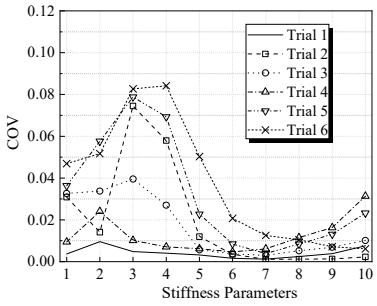

Fig. 10 COVs of stiffness parameters for the sensor failure case

and the corresponding resultant COVs of the stiffness parameters are shown in Fig. 10. For a given sensor configuration, the information gained from the measurements reduces due to sensor failure, and hence its estimation accuracy decreases. As expected, the overall estimation accuracy of Trial 1 is the best among all the six trials. Except for the optimal robust wireless sensor network configuration, the maximum COVs of all the estimated parameters of the other five trials exceed 1%. The maximum COV of parameters of Trial 2 is 7.8 times of that of Trial 1. It is observed that except Trial 5, the terminated sensing channels of the other trials are cluster head nodes. Trial 2 and 6 lost four sensing channels. Trial 1 and 3 lost three sensing channels. Trial 4 and 5 lost one sensing channel. Although the number of lost channels of Trial 1 is more than that of Trial 4 and Trial 5, its estimation accuracy is still the highest. This confirmed that the identification effectiveness of the optimal design obtained by the proposed method is robust against sensor failure.

6.2 Example 2: Bridge Model

A bridge model (shown in Fig. 11) is considered in the second example. The geometry and material properties of the bridge are listed in Table 6. The first five nominal natural frequencies are 0.116, 0.240, 0.318, 0.393 and 0.443 Hz. The damping matrix is taken as $\mathbf{C} = \alpha\mathbf{M} + \beta\mathbf{K}$, where α and β are 9.829×10^{-3} s^{-1} and 0.0089, respectively. As a result, the damping ratios of the first two modes are 1%. The bridge was subjected to horizontal and vertical excitations, which were modeled as zero-mean Gaussian white noise with a spectral intensity 5.0×10^{-4} m^2/s^3.

Twelve stiffness parameters in $\boldsymbol{\theta} = [\theta_{k1}, \theta_{k2}, \theta_{k3}, \theta_{k4}, \theta_{k5}, \theta_{k6}, \theta_{k7}, \theta_{k8}, \theta_{k9}, \theta_{k10}, \theta_{k11}, \theta_{k12}]^T$ are used to characterize the stiffness matrix $\mathbf{K}$. As shown in Fig. 11, the elements of the bridge are divided into twelve parts and each element is governed by one stiffness parameter. A multi-type sensory system that contains displacement transducers and accelerometers was installed. The electronic energy coefficient for data transmission, data reception and data aggregation are $e_T = 45$ nJ/bit, $e_R = 135$ nJ/bit and $e_A = 5$ nJ/bit/signal, respectively. The cluster radius is $R_c = 150$ m; the number of bits per packet for displacement transducers is 3200 bits/s; and the number of bits per packet for accelerometers is 4800 bits/s.

Table 6 Information about the bridge

Parameter	Value
Element length of deck (m)	50
Element length of pier (m)	20
Cross-sectional area of deck (m^2)	3.84
Cross-sectional area of pier (m^2)	3.14
Mass density (kg/m^3)	2500
Young's modulus (Pa)	3×10^{10}

For comparison, two cases with different constrain conditions on the number of wireless sensors are discussed. In Case A, the overall number of sensors is fixed but there is no constraint on the number of sensors in all types. In Case B, the amount of displacement transducers is less than that of accelerometers (i.e., $0 < N_1 < \mathrm{INT}\left(\frac{N_L}{2}\right)$ and $\mathrm{INT}\left(\frac{N_L}{2}\right) < N_2 < N_L$, where N_L is the total number of sensors and $\mathrm{INT}(\cdot)$ takes the integer of a number).

6.2.1 Case A: No constraint on the number of sensors in all types

The allowable COV value of the estimated parameters is 1%. The optimal configuration without the consideration of sensor failure is conducted for comparison. Figs. 12 and 13 show the results of the optimal configurations with twelve, fourteen, and sixteen sensors of the proposed method and the method without the consideration of sensor failure, respectively. The white and shaded circular node represent the displacement transducer and accelerometer, respectively. The data transmission route from a non-cluster head node to a cluster head node is represented by a dotted arrow while the route from a cluster head node to the base station is represented by a solid arrow. It is observed that the two methods provide different optimal designs. For example, when twelve sensors are available, the optimal design of the proposed method and the method without the consideration of sensor failure are shown in Fig. 12(a) and Fig. 13(a), respectively. According to the proposed method, seven displacement transducers are placed at the x-direction of the 31st node and the y-direction of the 5th, 8th, 14th,

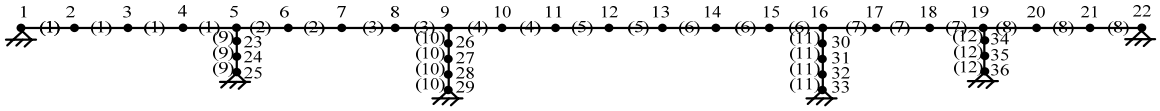

Fig. 11 Bridge model

Table 7 Resultant properties of the optimal configurations (Case A)

No. of sensors	Design					
	Proposed robust design			Design without considering sensor failure		
	E(J/h)	$\zeta_{\mathbf{L}}^{\mathcal{M}}$	$\zeta_{\mathbf{L}}^{\mathcal{MR}}$	E(J/h)	$\zeta_{\mathbf{L}}^{\mathcal{M}}$	$\zeta_{\mathbf{L}}^{\mathcal{MR}}$
12	89.28	0.90%	0.96%	65.80	0.99%	3.81%
14	92.52	0.81%	0.91%	77.41	0.96%	2.26%
16	113.04	0.80%	0.88%	107.64	0.91%	3.75%

15th, 16th and 19th node. In addition, five accelerometers are placed at the x-direction of the 26th and 27th node and the y-direction of the 8th, 9th and 13th node. On the other hand, according to the optimal design without the consideration of sensor failure, eight displacement transducers are placed at the x-direction of the 30th node and the y-direction of the 6th, 8th, 9th, 11th, 16th, 18th, and 19th node. Besides, four accelerometers are placed at the x-direction of the 27th node and the y-direction of the 7th, 10th and 13th node. This reconfirmed that the optimal sensor configuration without the consideration of sensor failure is no longer optimal due to the presence of sensor failure.

It is found that the number of the accelerometers is less than or equal to the number of the displacement transducers regardless of the optimization methods. Compared to the accelerometer, the displacement transducer transfers fewer bits per packet so that it consumes less energy under the same transmission distance. However, for both methods,

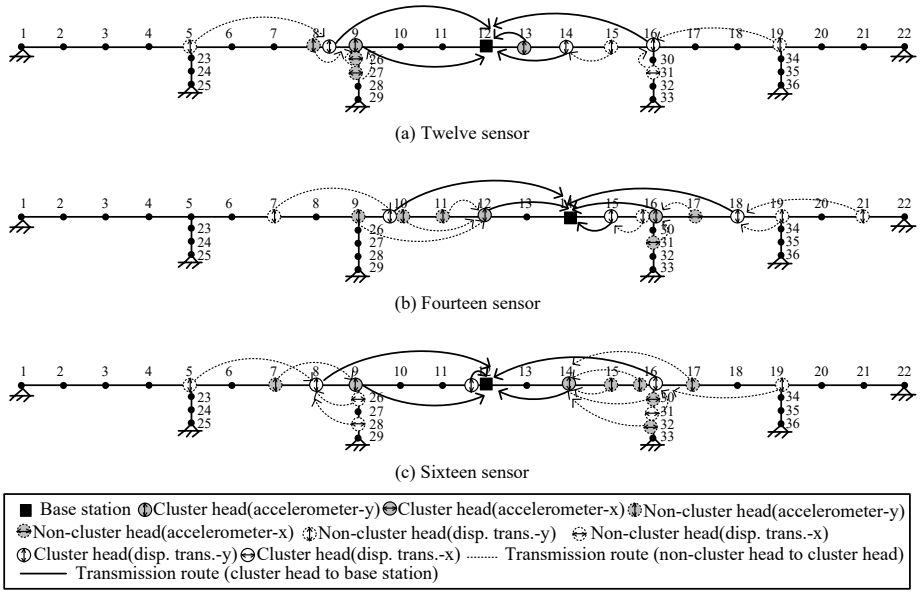

Fig. 12 Optimal robust wireless sensor network configurations by proposed method (Case A)

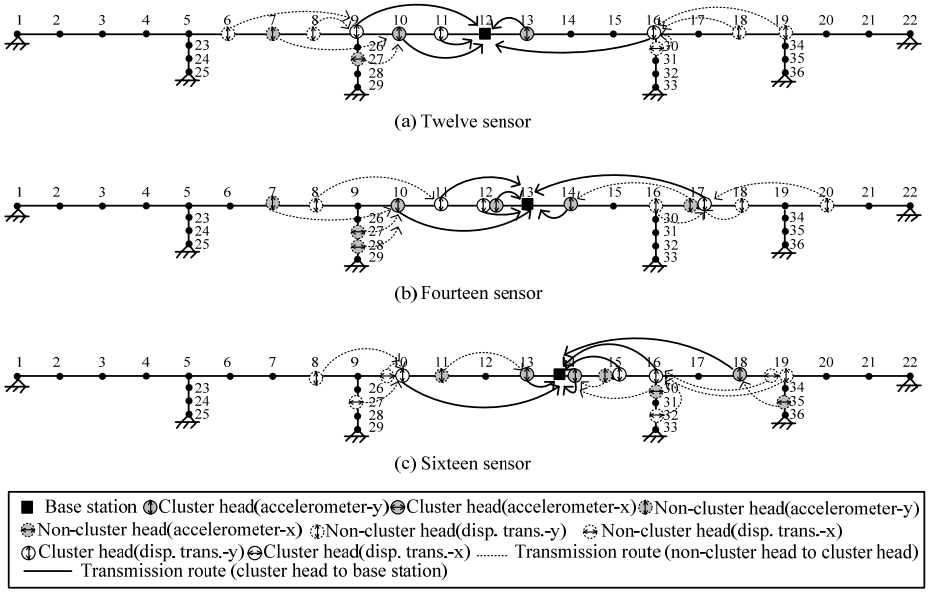

Fig. 13 Optimal wireless sensor network configurations without the consideration of sensor failure (Case A)

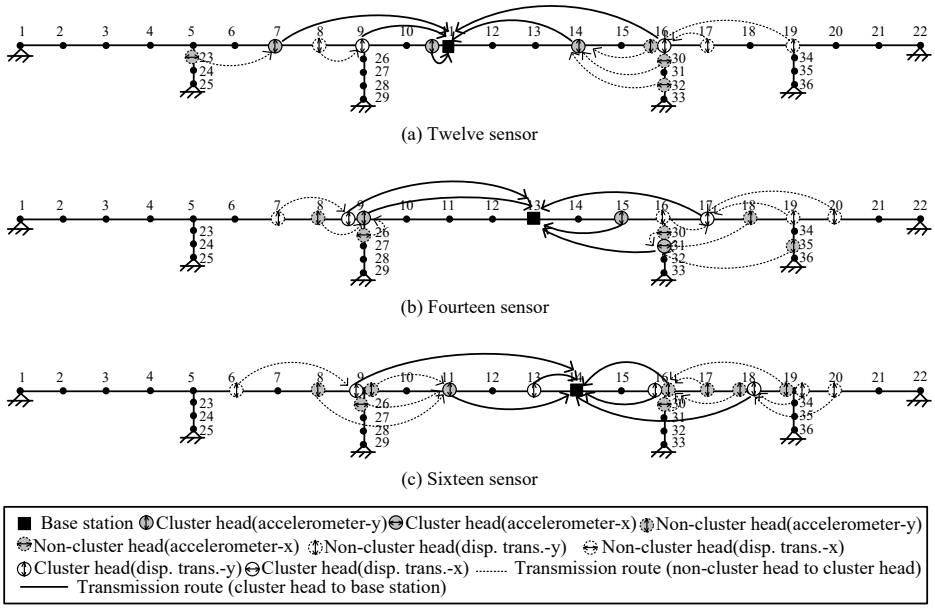

Fig. 14 Optimal robust wireless sensor network configurations by proposed method (Case B)

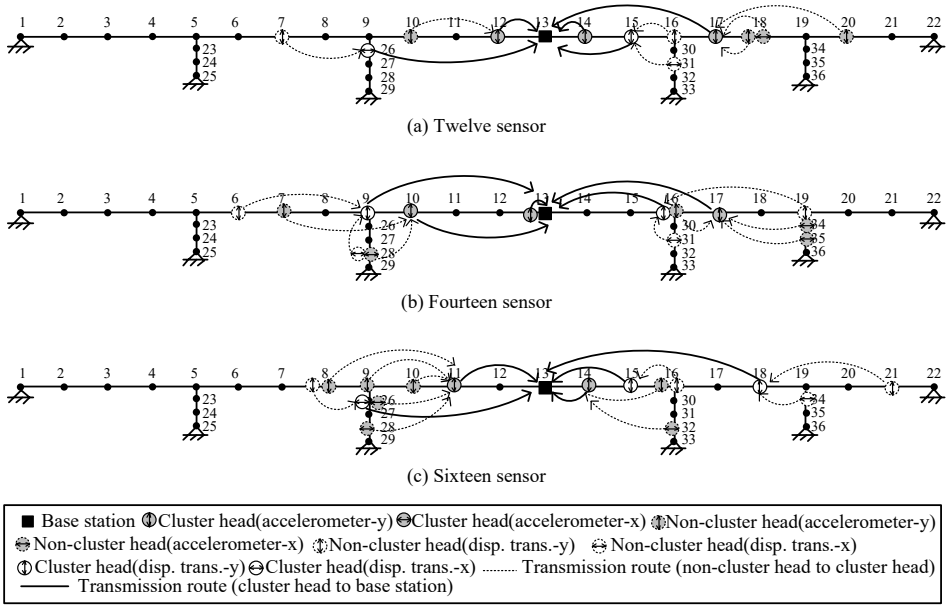

Fig. 15 Optimal wireless sensor network configurations without the consideration of sensor failure (Case B)

if only accelerometers are used to monitor the structural response, the estimation accuracy of the optimal design will be superior to that of Case A but the corresponding energy consumption will be larger. Consequently, the estimation accuracy of the optimal sensor configuration obtained by considering both the information effectiveness and energy consumption is lower than that of the optimal design determined based on the information effectiveness only.

Moreover, it is found that the displacement response in the y-direction of node 16 is crucial. This sensor is involved in all the optimal sensor configurations of both methods. The three optimal robust wireless sensor network configurations contain some common sensors which are the accelerometer in the y-direction of the 9th node and the displacement transducers in the y-direction of the 16th and 19th node. Furthermore, there are five clusters in the three optimal robust wireless sensor network configurations. However, without considering sensor failure, the optimal configuration with twelve sensors has five clusters while the optimal configurations with fourteen and sixteen sensors have six clusters.

The resultant energy consumption, maximum COVs, and robust maximum COVs are shown in Table 7. It is obvious that the consumed energy of the optimal design increases as more sensors are involved. With the same number of sensors, the consumed energy of the optimal configuration without the consideration of sensor failure is lower than that of the optimal robust wireless sensor network configuration. When any sensors become malfunction, the information gained from the measurement

reduces. Therefore, the robust maximum COVs $\zeta_{\mathbf{L}}^{\mathcal{M}R}$ are larger than the maximum COVs $\zeta_{\mathbf{L}}^{\mathcal{M}}$. When all sensors are well-functioning, all the resultant values of $\zeta_{\mathbf{L}}^{\mathcal{M}}$ by both methods do not exceed the allowable value 1%. However, the robust maximum COVs of the optimal design without the consideration of sensor failure no longer fulfill the accuracy requirement. The estimation accuracy of the optimal robust wireless sensor network configuration deteriorates milder than that obtained without considering sensor failure. It indicates that the proposed optimal robust configuration is more robust against sensor failure. The results show that the proposed method successfully develops the energy-efficient configuration that satisfies the required estimation accuracy even the networks contain malfunctioned sensors.

6.2.2 Case B: More accelerometers than displacement transducers

In Case B, the lower and upper bounds of the number of displacement transducers and accelerometers are specified as $0 < N_1 < \text{INT}\left(\frac{N_L}{2}\right)$ and $\text{INT}\left(\frac{N_L}{2}\right) < N_2 < N_L$, respectively. Figs. 14 and 15 show the results of the optimal configurations with twelve, fourteen, and sixteen sensors of the proposed method and the method without the consideration of sensor failure, respectively. As shown in these two figures, the displacement transducer in the y-direction of the 16th node is involved in all the optimal configurations. On the other hand, some sensors are selected in both cases only under a fixed number of sensors. For example, for the optimal designs with twelve sensors, the displacement transducers in the y-direction of the 8th, 16th and 19th nodes are involved in both cases. However, the displacement transducer in the y-direction of the 8th node is excluded in the optimal configuration with fourteen sensors in both cases. The optimal robust wireless sensor network configurations with twelve and fourteen sensors of Case B contain the same number of clusters as those of Case A. The optimal robust wireless sensor network configuration becomes six clusters when sixteen sensors are involved.

Table 8 shows the resultant energy consumption, maximum COVs, and robust maximum COVs of the optimal designs of Case B. Again, when the networks contain malfunctioned sensors, the optimal robust wireless sensor network configuration provides higher estimation accuracy compared to the optimal configuration without the consideration of sensor failure. For a given number of sensors, the energy consumption of the optimal robust wireless sensor network configurations of Case B is larger than that of Case A. It is because fewer possible configurations can be implemented in the optimization due to the imposed constraints. For example, the energy consumption of the optimal robust configuration with twelve sensors of Case A is 89.28 J/h and that of Case B is 138.32 J/h. This example demonstrates that the proposed method provides the optimal robust configuration of versatile wireless sensor networks. The resultant optimal design is robust against sensor failure. Moreover, it achieves the minimum energy consumption that satisfies the required estimation accuracy.

Table 8 Resultant properties of the optimal configurations (Case B)

No. of sensors	Design					
	Proposed robust design			Design without considering sensor failure		
	E(J/h)	$\zeta_{\mathbf{L}}^{\mathcal{M}}$	$\zeta_{\mathbf{L}}^{\mathcal{M}R}$	E(J/h)	$\zeta_{\mathbf{L}}^{\mathcal{M}}$	$\zeta_{\mathbf{L}}^{\mathcal{M}R}$
12	138.32	0.88%	0.91%	93.53	0.95%	1.58%
14	138.96	0.76%	0.99%	122.04	0.94%	1.97%
16	147.96	0.71%	0.99%	138.42	0.91%	2.17%

7. Conclusions

This paper presented an energy-aware robust wireless sensor network configuration design method with the consideration of possible sensor failure. The resultant optimal robust configuration achieves the required estimation accuracy with the minimal energy cost. By implementing Bayesian inference, the robust maximum coefficient of variation (COV) of the estimated parameters can be obtained to quantify the estimation accuracy of various sensor configurations with malfunctioned sensors. The three major features of the proposed method are: (1) possible malfunctioned sensors are considered to develop the robust sensor network configuration; (2) versatile types of sensors can be evaluated in a holistic manner; and (3) the resultant design achieves the required estimation accuracy with the minimum energy consumption. The illustrative examples demonstrated that the designed wireless sensor network configuration is robust against sensor failure. The proposed method selects the most energy-efficient sensor network configuration that satisfies the required estimation accuracy. The network configuration can be affected by the data transmission modes. Our future work will explore the network configuration design with flexible data transmission modes.

Acknowledgments

This work is funded by the Science and Technology Development Fund, Macau SAR under Research Grant SKL-IOTSC(UM)-2021-2023 and 0094/2021/A2, the Research Committee of University of Macau under Research Grant MYRG2018-00048-AAO and SRG2021-00006-FST, and the Guangdong-Hong Kong-Macau Joint Laboratory Program under Grant 2020B1212030009. These generous supports are gratefully acknowledged.

References

Al-Turjman, F.M., Hassanein, H.S. and Ibnkahla, M. (2015), "Towards prolonged lifetime for deployed WSNs in outdoor environment monitoring", *Ad. Hoc. Netw.*, **24**, 172-185. https://doi.org/10.1016/j.adhoc.2014.08.017

Argyris, C., Chowdhury, S., Zabel, V. and Papadimitriou, C.

(2018), "Bayesian optimal sensor placement for crack identification in structures using strain measurements", *Struct. Control. Health. Monit.*, **25**(5), e2137. https://doi.org/10.1002/stc.2137

Aswal, N., Sen, S. and Mevel, L. (2022), "Switching Kalman filter for damage estimation in the presence of sensor faults", *Mech. Syst. Signal. Process.*, **175**, 109116. https://doi.org/10.1016/j.ymssp.2022.109116

Bhuiyan, M.Z.A. and Cao, J.N. (2015), "Deploying wireless sensor networks with fault-tolerance for structural health monitoring", *IEEE Trans. Comput.*, **64**, 382-395. https://doi.org/10.1109/TC.2013.195

Casciati, F. and Fuggini, C. (2011), "Monitoring a steel building using GPS sensors", *Smart. Struct. Syst.*, *Int. J.*, **7**(5), 349-363. https://doi.org/10.12989/sss.2011.7.5.349

El-Qawasma, F.A., Elfouly, T.M. and Ahmed, M.H. (2019), "Minimising number of sensors in wireless sensor networks for structure health monitoring systems", *IET. Wireless. Sensor Syst.*, **9**(2), 94-101. https://doi.org/10.1049/iet-wss.2018.5031

Elhabyan, R., Shi, W. and St-Hilaire, M. (2019), "Coverage protocols for wireless sensor networks: review and future directions", *J. Commun. Netw.*, **21**(1), 45-60. https://doi.org/10.1109/JCN.2019.000005

Elsersy, M., Elfouly, T.M. and Ahmed, M.H. (2016), "Joint optimal placement, routing, and flow assignment in wireless sensor networks for structural health monitoring", *IEEE Sensors J.*, **16**(12), 5095-5106. https://doi.org/10.1109/JSEN.2016.2554462

Ercan, T. and Papadimitriou, C. (2021), "Optimal sensor placement for reliable virtual sensing using modal expansion and information theory", *Sensors*, **21**(10), 3400. https://doi.org/10.3390/s21103400

Ercan, T., Sedehi, O., Katafygiotis, L.S. and Papadimitriou, C. (2023), "Information theoretic-based optimal sensor placement for virtual sensing using augmented Kalman filtering", *Mech. Syst. Signal. Process.*, **188**, 110031. https://doi.org/10.1016/j.ymssp.2022.110031

Fang, K., Liu, C. and Teng, J. (2018), "Cluster-based optimal wireless sensor deployment for structural health monitoring", *Struct. Health. Monit.*, **17**(2), 266-278. https://doi.org/10.1177/1475921717689967

Fu, T.S., Ghosh, A., Johnson, E.A. and Krishnamachari, B. (2013), "Energy-efficient deployment strategies in structural health monitoring using wireless sensor networks", *Struct. Control. Health. Monitor.*, **20**(6), 971-986. https://doi.org/10.1002/stc.1510

Geoffrine, J.M.C. and Geetha, V. (2019), "Energy optimization with higher information quality for SHM application in wireless sensor networks", *IEEE Sensors J.*, **19**(9), 3513-3520. https://doi.org/10.1109/JSEN.2019.2892870

Hao, X.H., Yuen, K.V. and Kuok, S.C. (2022a), "Energy-aware versatile wireless sensor network configuration for structural health monitoring", *Struct. Control. Health. Monitor.*, **29**(11), e3083. https://doi.org/10.1002/stc.3083

Hao, X.H., Kuok, S.C. and Yuen, K.V. (2022b), "Wireless sensor network design for large-scale infrastructures health monitoring with optimal information-lifespan tradeoff", *Smart Struct. Syst.*, *Int. J.*, **30**(6), 583-599. https://doi.org/10.12989/sss.2022.30.6.583

Heinzelman, W.B., Chandrakasan, A.P. and Balakrishnan, H. (2002), "An application-specific protocol architecture for wireless microsensor networks", *IEEE Trans. Wirel. Commun.*, **1**, 660-670. https://doi.org/10.1109/TWC.2002.804190

Hu, Q.L., Liu, X., Wu, Q.B., Cao, J.N., Liu, Y. and Tan, Y.S. (2012), "Cluster-based energy-efficient structural health monitoring using wireless sensor networks", In: *International Conference on Computer Science & Service System* (*CSSS*), Nanjing, China, August.

Huang, K., Yuen, K.V., Wang, L., Jiang, T.Y. and Dai, L.Z. (2022), "Sensor fault detection, localization, and reconstruction for online structural identification", *Struct. Control. Health. Monitor.*, **29**(4), e2925. https://doi.org/10.1002/stc.2925

Huynh, T.C., Nguyen, T.D., Ho, D.D., Dang, N.L. and Kim, J.T. (2020), "Sensor fault diagnosis for impedance monitoring using a piezoelectric-based smart interface technique", *Sensors* (*Basel*), **20**(2), 510. https://doi.org/10.3390/s20020510

Jalsan, K.E., Rohan, N.S. and Flouri, K. (2014), "Layout optimization of wireless sensor networks for structural health monitoring", *Smart Struct. Syst.*, *Int. J.*, **14**(1), 39-54. https://doi.org/10.12989/sss.2014.14.1.039

Jana, D., Patil, J., Herkal, S., Nagarajaiah, S. and Duenas-Osorio, L. (2022), "CNN and Convolutional Autoencoder (CAE) based real-time sensor fault detection, localization, and correction", *Mech. Syst. Signal Process.*, **169**, 108723. https://doi.org/10.1016/j.ymssp.2021.108723

Jeong, S., Kim, H., Lee, J. and Sim, S.H. (2021), "Automated wireless monitoring system for cable tension forces using deep learning", *Struct. Health. Monitor.*, **20**(4), 1805-1821. https://doi.org/10.1177/1475921720935837

Kammer, D.C. (1991), "Sensor placement for on-orbit modal identification and correlation of large space structures", *J. Guid. Control Dyn.*, **14**(2), 251-259. https://doi.org/10.2514/3.20635

Katafygiotis, L.S. and Yuen, K.V. (2001), "Bayesian spectral density approach for modal updating using ambient data", *Earthq. Eng. Struct. Dyn.*, **30**(8), 1103-1123. https://doi.org/10.1002/eqe.53

Kuok, S.C. and Yuen, K.V. (2012), "Structural health monitoring of Canton Tower using Bayesian framework", *Smart Struct. Syst.*, *Int. J.*, **10**(4-5), 375-391. https://doi.org/10.12989/sss.2012.10.4_5.375

Lam, H.F. and Adeagbo, M.O. (2022), "An enhanced sequential sensor optimization scheme and its application in the system identification of a rail-sleeper-ballast system", *Mech. Syst. Signal Process.*, **163**, 108188. https://doi.org/10.1016/j.ymssp.2021.108188

Lam, H.F., Yang, J.H., Hu, Q. and Ng, T.C. (2018), "Railway ballast damage detection by Markov chain Monte Carlo-based Bayesian method", *Struct. Health. Monitor.*, **17**(3), 706-724. https://doi.org/10.1177/1475921717717106

Lei, Y., Yang, N. and Xia, D.D. (2017), "Probabilistic structural damage detection approaches based on structural dynamic response moments", *Smart Struct. Syst.*, *Int. J.*, **20**(2), 207-217. https://doi.org/10.12989/sss.2017.20.2.207

Lei, Y., Lu, J.B. and Huang, J.S. (2020), "Synthesize identification and control for smart structures with time-varying parameters under unknown earthquake excitation", *Struct. Control Health. Monitor.*, **27**(4), e2512. https://doi.org/10.1002/stc.2512

Lei, Y., Zhang, Y., Mi, J., Liu, W.F. and Liu, L.J. (2021), "Detecting structural damage under unknown seismic excitation by deep convolutional neural network with wavelet-based transmissibility data", *Struct. Health. Monitor.*, **20**(4), 1583-1596. https://doi.org/10.1177/1475921720923081

Li, B., Wang, D., Wang, F. and Ni, Y.Q. (2010), "High quality sensor placement for SHM systems: Refocusing on application demands", In: *INFOCOM'10*, *International Conference on IEEE*, San Diego, CA, USA, March.

Li, J., Hao, H. and Chen, Z. (2017), "Damage identification and optimal sensor placement for structures under unknown traffic-induced vibrations", *J. Aerosp. Eng.*, **30**(2), B4015001. https://doi.org/10.1061/(ASCE)AS.1943-5525.0000550

Li, L.L., Liu, G., Zhang, L.L. and Li, Q. (2019), "Sensor fault detection with generalized likelihood ratio and correlation coefficient for bridge SHM", *J. Sound. Vib.*, **442**, 445-458. https://doi.org/10.1016/j.jsv.2018.10.062

Liu, W., Gao, W.C., Sun, Y. and Xu, M.J. (2008), "Optimal sensor placement for spatial lattice structure based on genetic algorithms", *J. Sound Vib.*, **317**, 175-189. https://doi.org/10.1016/j.jsv.2008.03.026

Liu, X., Cao, J., Lai, S., Yang, C., Wu, H. and Xu, Y. (2011), "Energy efficient clustering for WSN-based structural health monitoring", *Proceedings of 30th IEEE International Conference on Computer Communications* (*INFOCOM*), Shanghai, China, April.

Liu, C., Jiang, Z., Wang, F. and Chen, H. (2016), "Energy-efficient heterogeneous wireless sensor deployment with multiple objectives for structural health monitoring", *Sensors*, **16**, 1865. https://doi.org/10.3390/s16111865

Noori, M., Cao, Y., Hou, Z.K. and Sharma, S. (2010), "Application of support vector machine for reliability assessment and structural health monitoring", *Int. J. Eng. Under. Uncertain.: Hazard. Assess. Mitig.*, **2**(3-4), 89-98.

Onoufriou, T., Soman, R.N., Votsis, R., Chrysostomou, C. and Kyriakides, M. (2012), "Optimization of wireless sensor locations for SHM based on application demands and networking limitations", In: *Management*, *Resilience and Sustainability*: *6th International Conference on Bridge Maintenance*, *Safety and Management*, Stresa, Lake Maggiore, Italy.

Papadimitriou, C. and Lombaert, G. (2012), "The effect of prediction error correlation on optimal sensor placement in structural dynamics", *Mech. Syst. Signal Process.*, **28**, 105-127. https://doi.org/10.1016/j.ymssp.2011.05.019

Papadopoulos, M. and Garcia, E. (1998), "Sensor placement methodologies for dynamic testing", *AIAA J.*, **36**(2), 256-263. https://doi.org/10.2514/2.7509

Reynier, M. and Abou-Kandil, H. (1999), "Sensors location for updating problems", *Mech. Syst. Signal Process.*, **13**(2), 297-314. https://doi.org/10.1006/mssp.1998.1213

Sengupta, S., Das, S. and Nasir, M.D. (2013), "Multi-objective node deployment in WSNs: In search of an optimal trade-off among coverage, lifetime, energy consumption, and connectivity", *Eng. Appl. Artif. Intell.*, **26**(1), 405-416. https://doi.org/10.1016/j.engappai.2012.05.018

Shi, Q., Wang, X., Chen, W. and Hu, K. (2020), "Optimal sensor placement method considering the importance of structural performance degradation for the allowable loadings for damage identification", *Appl. Math. Model.*, **86**, 384-403. https://doi.org/10.1016/j.apm.2020.05.021

Spencer, B.F. and Cho, S. (2011), "Wireless smart sensor technology for monitoring civil infrastructure: technological developments and full-scale applications", *Proceedings of the Advances in Structural Engineering and Mechanics* (*ASEM'11*), Seoul, Korea, September.

Spencer, B.F., Ruiz-Sandoval, M.E. and Kurata, N. (2004), "Smart sensing technology: opportunities and challenges", *Struct. Control Health Monitor.*, **11**(4), 349-368. https://doi.org/10.1002/stc.48

Stephan, C. (2012), "Sensor placement for modal identification", *Mech. Syst. Signal. Process.*, **27**, 461-470. https://doi.org/10.1016/j.ymssp.2011.07.022

Tan, Y. and Zhang, L.M. (2020), "Computational methodologies for optimal sensor placement in structural health monitoring: a review", *Struct. Health Monitor.*, **19**(4), 1287-1308. https://doi.org/10.1177/1475921719877579

Udwadia, F.E., (1994), "Methodology for optimal sensor locations for parameters identification in dynamic systems", *J. Eng. Mech.*, **120**(2), 368-390. https://doi.org/10.1061/(ASCE)0733-9399(1994)120:2(368)

Yao, L., Sethares, W.A. and Kammer, D.C. (1993), "Sensor placement for on-orbit modal identification via a genetic algorithm", *AIAA J.*, **31**(10), 1922-1928. https://doi.org/10.2514/3.11868

Yi, T.H., Li, H.N. and Gu, M. (2011), "Optimal sensor placement for health monitoring of high-rise structure based on genetic algorithm", *Math. Probl. Eng.*, **2011**, 395101. https://doi.org/10.1155/2011/395101

Yi, T.H., Yao, X.J., Qu, C.X. and Li, H.N. (2019), "Clustering number determination for sparse component analysis during output-only modal identification", *J. Eng. Mech.*, **145**(1). https://doi.org/10.1061/(ASCE)EM.1943-7889.0001557

Yuen, K.V. and Kuok, S.C. (2015), "Efficient Bayesian sensor placement algorithm for structural identification: a general approach for multi-type sensory systems", *Earthq. Eng. Struct. Dyn.*, **44**(5), 757-774. https://doi.org/10.1002/eqe.2486

Yuen, K.V., Katafygiotis, L.S., Papadimitriou, C. and Mickleborough, M.C. (2001), "Optimal sensor placement methodology for identification with unmeasured excitation", *Dyn. Syst. Measur. Contr.*, **123**(4), 677-686. https://doi.org/10.1115/1.1410929

Yuen, K.V., Hao, X.H. and Kuok, S.C. (2022), "Robust sensor placement for structural identification", *Struct. Control Health Monitor.*, **29**(1), e2861. https://doi.org/10.1002/stc.2861

Zhang, F.L., Ni, Y.C., Au, S.K. and Lam, H.F. (2016), "Fast Bayesian approach for modal identification using free vibration data, Part I - Most probable value", *Mech. Syst. Signal Process.*, **70-71**, 209-220. https://doi.org/10.1016/j.ymssp.2015.05.031

Zhang, F.L., Yang, Y.P., Ye, X.W., Yang, J.H. and Han, B.K. (2019), "Structural modal identification and MCMC-based model updating by a Bayesian approach", *Smart Struct. Syst., Int. J.*, **24**(5), 631-639. https://doi.org/10.12989/sss.2019.24.5.631

Zhang, Y.X., Wang, X.Y., Ding, Z.H., Du, Y. and Xia, Y. (2022), "Anomaly detection of sensor faults and extreme events based on support vector data description", *Struct. Control Health Monit.*, **29**(10), e3047. https://doi.org/10.1002/stc.3047

Zhang, Z.F., Peng, C., Wang, G.J., Ju, Z.Y. and Ma, L. (2023), "Optimal sensor placement for strain sensing of a beam of high-speed EMU", *J. Sound. Vib.*, **542**, 117359. https://doi.org/10.1016/j.jsv.2022.117359

Zhao, Y., Noori, M., Altabey, W.A. and Beheshti-Aval, S.B. (2018), "Mode shape-based damage identification for a reinforced concrete beam using wavelet coefficient differences and multiresolution analysis", *Struct. Control Health Monitor.*, **25**(1), e2041. https://doi.org/10.1002/stc.2041

Zhou, G.D. and Yi, T.H. (2013), "Recent developments on wireless sensor networks technology for bridge health monitoring", *Math. Probl. Eng.*, **3**, 1-33. https://doi.org/10.1155/2013/947867

Zhou, G.D., Yi, T.H. and Zhang, H. (2015), "Energy-aware wireless sensor placement in structural health monitoring using hybrid discrete firefly algorithm", *Struct. Control Health Monit.*, **22**, 648-666. https://doi.org/10.1002/stc.1707

Zhou, G.D., Xie, M.X., Yi, T.H. and Li, H.N. (2019), "Optimal wireless sensor network configuration for structural monitoring using automatic-learning firefly algorithm", *Adv. Struct. Eng.*, **22**(4), 907-918. https://doi.org/10.1177/1369433218797074

Zhou, G.D., Yi, T.H., Xie, M.X., Li, H.N. and Xu, J.H. (2021), "Optimal wireless sensor placement in structural health monitoring emphasizing information effectiveness and network performance", *J. Aerosp. Eng.*, **34**(2), 04020112. https://doi.org/10.1061/(ASCE)AS.1943-5525.0001226

Zhou, X., Zhang, F.L., Goi, Y. and Kim, C.W. (2023), "Bayesian model update for damage detection of a steel plate girder bridge", *Smart Struct. Syst., Int. J.*, **31**(1), 29-43. https://doi.org/10.12989/sss.2023.31.1.029